CoFAR Clutter Estimation using Covariance-Free Bayesian Learning

Kunwar Pritiraj Rajput, ***Member, IEEE***
Interdisciplinary Centre for Security, Reliability and Trust (SnT), University of Luxembourg, Luxembourg City L-1855, Luxembourg

Bhavani Shankar M. R., ***Senior Member, IEEE***
Interdisciplinary Centre for Security, Reliability and Trust (SnT), University of Luxembourg, Luxembourg City L-1855, Luxembourg

Kumar Vijay Mishra, ***Senior Member, IEEE***
United States DEVCOM Army Research Laboratory, Adelphi, MD 20783 USA

Muralidhar Rangaswamy, ***Fellow, IEEE***
United States Air Force Research Laboratory, Wright-Patterson Air Force Base, Ohio, USA

Björn Ottersten, ***Fellow, IEEE***
Interdisciplinary Centre for Security, Reliability and Trust (SnT), University of Luxembourg, Luxembourg City L-1855, Luxembourg

***Abstract*— A cognitive fully adaptive radar (CoFAR) adapts its behavior on its own within a short period of time in response to changes in the target environment. For the CoFAR to function properly, it is critical to understand its operating environment through estimation of the clutter channel impulse response (CCIR). In general, CCIR is sparse but prior works either ignore it or estimate the CCIR by imposing sparsity as an explicit constraint in their optimization problem. In this paper, contrary to these studies, we develop covariance-free Bayesian learning (CoFBL) techniques for estimating sparse CCIR in a CoFAR system. In particular, we consider a multiple measurement vector scenario and estimate a simultaneously sparse (row sparse) CCIR matrix. Our CoFBL framework reduces the complexity of conventional sparse Bayesian learning through the use of the diagonal element estimation rule and conjugate gradient descent algorithm. We show that the framework is applicable to various forms of CCIR sparsity models: group, joint, and joint-cum-group. We evaluate our method through numerical experiments on a data set generated using RFView®, a high-fidelity modeling and simulation tool. We derive Bayesian Cramér-Rao bounds for the various considered scenarios to benchmark the performance of our algorithms. Our results demonstrate that the proposed CoFBL-based approaches perform better than the existing popular approaches such as multiple focal underdetermined system solver and simultaneous orthogonal matching pursuit.**

***Index Terms*— Bayesian Cramér-Rao bound, clutter map, cognitive fully adaptive radar, RFView®, sparse Bayesian learning.**

This research was funded in whole, or in part, by the Luxembourg National Research Fund (FNR), grant reference 18014377, SENCOM under Grant C20/IS/14799710/SENCOM and METSA project under Grant C22/IS/17391632. For the purpose of open access, and in fulfillment of the obligations arising from the grant agreement, the author has applied a Creative Commons Attribution 4.0 International (CC BY 4.0) license to any Author Accepted Manuscript version arising from this submission. This work from the University of Luxembourg is partially supported by the grant on "Active Learning for Cognitive Radars" from the European Office of Aerospace Research Development, part of the US Airforce Office of Scientific Research. K. P. R., M. R. B. S., and B. O. are with the interdisciplinary center of security reliability and trust (SnT), University of Luxembourg, 1855, Luxembourg (e-mail: {kunwar.rajput, bhavani.shankar, bjorn.ottersten}@uni.lu). K. V. M. is with the United States DEVCOM Army Research Laboratory, Adelphi, Maryland, USA (e-mail: kvm@ieee.org). M. R. is with the United States Air Force Research Laboratory, Wright-Patterson Air Force Base, Ohio, USA (email:muralidhar.rangaswamy@us.af.mil). The conference precursor to this work [1] was published in the 2023 IEEE Radar Conference (RadarConf).

I. Introduction

A cognitive fully adaptive radar (CoFAR) accumulates the knowledge of the target environment and subsequently, optimizes its transmit and receive functions adaptively for enhanced performance [2–5]. The purpose of adaptive processing may include desired results such as target identification [6] and tracking [7]. Conventional radars use a feed-forward mechanism, which transfers raw detected data to a higher-level processor for more sophisticated functions. The FAR system, on the other hand, uses a feedback mechanism and optimization criteria to enhance sensing in the following scans. In the case of a multi-function radar that performs both detection and imaging, the optimization may have additional goals such as tracking, imaging, and classification [8]. Hardware prototypes that address certain FAR goals have also been exhibited. For instance, [9] designed a FAR system for target tracking in a non-linear range measurement model. In this paper, we focus on clutter channel impulse response (CCIR) estimation in the context of CoFAR.

To effectively analyze the target environment, it is important to estimate CCIR [10, 11], which is made up of undesirable echoes including ground reflections, atmospheric effects, and electromagnetic interference [12–17]. These factors hinder radar performance by reducing detection and estimation capabilities [18]. Kay in [18] proposed an optimal signal design for a Gaussian single target in the presence of clutter which is also modeled as Gaussian random process (GRP). In space time adaptive processing (STAP) the traditional clutter model establishes a non-linear relationship between the signal-dependent covariance and the transmit radar waveform, making it difficult to accurately estimate the signal-dependent clutter covariance matrix. However, the multi-input multi-output (MIMO) clutter model proposed in [19] employs a "stochastic transfer function" to overcome this issue. This transfer function is derived from a physical scattering model and may be viewed as a stochastic Green's function [20]. Although the complex clutter returns are influenced by the transmit signal, the stochastic transfer function is signal-independent. This

approach allows for joint optimization of the transmit waveform and receiver filters because the received signal is the convolution of the transmit waveform with the target and CCIRs.

For the waveform design problem, [19] presents an analytical solution that requires estimation from representative training data in practice. However, the accuracy of the channel transfer function estimates heavily influences the performance of this method. To address this issue, a low-complexity frequency-domain technique was proposed in [21] for estimating the channel matrix. This estimate is then incorporated into an optimization problem thereby allowing for the simultaneous design of the radar transmit-receive functions to achieve the CoFAR goal. Although this technique is easily implemented in real-time hardware, accurately estimating the CIR at low signal-to-noise ratio (SNR) levels requires probing signals with larger pulse-widths. This calls for a significant allocation of CoFAR resources thereby rendering this approach undesirable.

CoFAR performance is critically dependent on the knowledge of the CCIR [22–25]. Devoting CoFAR resources in order to gain that knowledge takes away from the radar dwell time for the primary surveillance function. Therefore, one has to exercise caution in terms of how often and how to probe the environment. Thus, exploiting structure inherent to the CCIR such as sparsity or constancy along certain band like constrained CCIR [23–25] helps in gaining that knowledge with less CoFAR resources. This affords a significant performance improvement by cutting down on the radar dwell time. To efficiently use CoFAR resources, it would be beneficial to take advantage of inherent structural details or relationships between nearby channel transfer functions in the estimation problem. To this end, [22, 23] exploit the fact that CIRs of neighboring pulses are often strongly correlated. This allows for the use of a constrained maximum likelihood (ML) estimate employing a cosine similarity constraint. However, the resulting optimization problems are semidefinite program (SDP) and second order cone program (SOCP) which entails high computational complexity. In [24], a constrained CIR estimation (CCIRE) was introduced which utilized both a cosine similarity constraint and sparsity in CIR. However, implementing this optimization method would also results in a computationally expensive SDP. Taking this paradigm forward, [25] developed a framework that exploits the cosine similarity and conducts experiments on the RFView®-generated real data sets.

An alternative approach to tackling the estimation problem involves leveraging a sparse signal recovery technique, such as Basis Pursuit [26] or the FOCal Underdetermined System Solver (FOCUSS) [27], to estimate the sparse CCIR. However, these methods come with fixed priors and are susceptible to structural and convergence errors. Moreover, they necessitate the tuning parameter λ to be determined through another method or set based on prior knowledge. Any disparity between the assumed prior and the data may lead to a substantial loss in performance. Structural errors escalate when the global minimum of the cost function is not the sparsest solution, and convergence errors arise when the method converges to a sub-optimal local minimum. In contrast, the sparse Bayesian learning (SBL) framework [28] has garnered considerable research attention as a tool for estimating the unknown sparse quantity while offering superior performance guarantees. Its application for simultaneously estimating sparse parameters was further extended in [29]. SBL has found application in various fields, including biomedical signal processing [30] and array processing [31, 32].

The parameterized prior in SBL does not require to tweak unknown regularization parameter. Moreover, it uses a tractable expectation maximization (EM) framework, which yields maximally sparse solution [28]. In the absence of noise, the global minimum occurs at the sparsest solution and there are no structural errors. For noisy signals, SBL performs reasonably well since the SBL cost function also has fewer local minima than the FOCUSS objective function, making it less susceptible to convergence errors [28].

The EM algorithm poses increased computational complexity due to the necessity of inverting a posterior covariance matrix. To mitigate this complexity, alternative algorithms based on Approximate Message Passing (AMP) [33] and Gaussian Belief Propagation (GBP) [34] can be employed. These approaches aim to reduce computational demands by conducting T_{amp} and T_{gbp} inner steps within each E-Step, estimating means and variances of the sparse parameters without resorting to matrix inversion. However, it's worth noting that AMP and GBP may encounter convergence issues, particularly in cases involving the estimation of variances [35]. An instance is when the dictionary fails to satisfy zero-mean and sub-Gaussian (i.e., distribution with a strong tail decay) criteria [36].

A different approach involves incorporating variational inference, aiming to approximate the actual posterior using a more manageable surrogate [37–39]. This technique facilitates inverse-free Sparse Bayesian Learning (SBL) inference [40, 41]. However, variational inference methods optimize a lower bound on the likelihood function rather than the true objective, potentially leading to convergence on a sub-optimal solution for the sparse quantity in question. In the context of this study, we also tackle the challenge of reducing the computational complexity of the Expectation-Maximization (EM) algorithm by eliminating the need for inverting the posterior covariance matrix in each EM iteration.

A. Our Contributions

Preliminary results of our work appeared in our conference publication [1], where we proposed a sparse CCIR vector estimation technique using conventional SBL [28] for a single-input multiple-output (SIMO) CoFAR system.

Table I

Canvas of the contributions of the current work vis-a-vis the state-of-the-art.

q.v.	Radar type	Antenna geometry	Measurements	Estimation method	Clutter model	Sparsity	Priors	Simulation tool
[1]	CoFAR	SIMO	SMV	Bayesian	Green's function	Standard	Not required	RFView
[3]	CoFAR	MIMO	SMV	Least Square	Delay-Doppler	No	N/A	Simulated
[5]	CoFAR	MIMO	SMV	STAP	Covariance based	No	N/A	Simulated
[17]	Conventional	SISO	SMV	Bayesian	GRP	No	N/A	Simulated
[20]	CoFAR	MIMO	SMV	Frequency domain	Green's function	No	N/A	RFView
[21]	CoFAR	MIMO	SMV	SDP	Green's function	No	N/A	RFView
[22]	CoFAR	MIMO	SMV	SOCP	Green's function	No	N/A	RFView
[23]	CoFAR	MIMO	SMV	SDP	Green's function	Standard	Yes	RFView
This paper	CoFAR	MIMO	MMV	Bayesian	Green's function	Standard, joint, group, joint-cum-group	Not required	RFView

[1] N/A: Not applicable.

This required only a single measurement vector model. In this paper, our main contributions are:

- **MIMO CoFAR:** We consider a multiple measurement vector (MMV) scenario and derive the SBL-based framework for the CCIR matrix estimation for a MIMO CoFAR. The proposed algorithm exploits the simultaneous or row sparsity in the range domain using the MMV framework. Prior works [1, 3, 5, 21–24] relied on single measurement vector (SMV) models.
- **Reduced computations in EM algorithm:** We develop the covariance-free Bayesian learning (CoFBL) framework [42] for the MMV model to substantially reduce the computational requirement of the E-step which requires the inversion of the covariance matrix. This requires computation of the diagonal elements of the posterior covariance matrix along with the posterior mean. Conventionally, this entails the inversion of the posterior covariance matrix but we avoid it using the diagonal estimation rule [43] together with conjugate gradient descent (CGD) algorithm [44] to solve linear system of equations.
- **Joint, group, and joint-cum-group sparse models:** We leverage upon the various sparse models of the underlying channel and develop covariance-free group (CoFGBL), joint (CoFJBL) and joint-cum-group Bayesian learning (CoFJGBL) techniques. This requires the computation of fewer hyperparameters and still yields a better estimation performance.
- **Comparisons with realistic datasets:** Previous related works [18, 45, 46] rely on simplified or highly theoretical models for datasets. We employ the high-fidelity modeling and simulation software RFView® to realistically evaluate our methods against the state-of-the-art.
- **Bayesian error bounds:** To benchmark the results, we derive Bayesian Cramér-Rao bounds (BCRBs) for various algorithms proposed in this work. We build upon the deterministic BCRB and specialize it to particular cases of interest for radar channel estimation. These scenarios rely on the identification of structures not exploited hitherto.

Table I summarizes our contributions with respect to state-of-the-art.

B. Organization and Notation

The rest of the paper is structured as follows. In the next section, we introduce the MMV system model for MIMO CoFAR. Section III describes the BL-based CCIR estimation algorithm using the conventional sparse BL (SBL) algorithm. In Section IV, we develop the low-complexity CoFBL framework for CCIR estimation. Then, we expand this in Section V to the proposed CoFGBL, CoFJBL, CoFJGBL methods. In Section VI, we derive the BCRBs for the different scenarios considered in this paper. We validate our models and methods through numerical experiments in Section VII and conclude in Section VIII followed by appendices.

Lowercase and uppercase bold letters represent vectors and matrices, respectively. The superscripts T and H denote transpose and Hermitian (conjugate transpose) operations, respectively. The statistical expectation and trace operator are defined as $\mathbb{E}[.]$ and $\mathrm{Tr}[.]$, respectively. The expression $\mathbf{x} \sim \mathcal{CN}(\boldsymbol{\mu}, \boldsymbol{\Sigma})$ represents a complex vector $\mathbf{x}$ with mean $\boldsymbol{\mu}$ and covariance matrix $\boldsymbol{\Sigma}$. The n-th element of a vector $\mathbf{x}$ is denoted by $\mathbf{x}(n)$, and the (n,n)-th element of a matrix $\mathbf{X}$ is denoted as $\mathbf{X}(n,n)$. The i-th row and j-th column of any matrix $\mathbf{X}$ are denoted as $\mathbf{X}_{i.}$ and $\mathbf{X}_{.j}$, respectively. The operation $\mathbf{vec}(.)$ converts an $n \times n$ matrix $\mathbf{X}$ into an $n^2 \times 1$ vector by performing column-wise stacking. The expression $\mathbf{X} = \mathrm{diag}[x_1, x_2, \ldots, x_N] \in \mathbb{C}^{N \times N}$ represents a diagonal matrix with elements $x_i \in \mathbb{C}$, $i = 1, 2, \ldots, N$ on its main diagonal. Finally, $*$ and $\odot$ ($\oslash$) denote the convolution, element-wise multiplication (division), respectively.

II. System Model

Consider a MIMO radar with N transmit and M receive antenna elements arranged in an uniform linear array (ULA) configuration with inter-element spacing d_T and d_R, respectively. The inter-element spacing of the transmit array admits values higher than half-wavelength without suffering from ambiguity at the receiver [47]. Therefore, we consider $d_R = \lambda/2$ so that $d_T = M\lambda/2$. The total aperture of the transmit and receive arrays is Z_t and Z_r, respectively. Denote $Z = Z_t + Z_r$. Then, the locations of n-th transmit and m-th receive antennas on the x-axis are $\frac{Znd_T}{2}$ and $\frac{Zmd_R}{2}$, respectively. At each

transmitter n, the transmit radar signal $x_n(t)$ is

$$x_n(t) = s_n(t)e^{j2\pi f_c t}, \tag{1}$$

where f_c is carrier frequency and $s_n(t)$ is a linear frequency modulated (LFM) baseband waveform

$$s_n(t) = A_n e^{\mathrm{j}2\pi\beta_n t^2}\,\mathrm{rect}\left(\frac{t}{T}\right),\ 0 < t < T, \tag{2}$$

where A_n is the signal amplitude, $\beta_n = \frac{B_n}{2T}$ is the ramp rate, B_n is the non-overlapping signal bandwidth of n-th transmit signal, and

$$\mathrm{rect}(t) = \begin{cases} 1, & 0 \le t < 1 \\ 0, & \text{otherwise}, \end{cases} \tag{3}$$

is the rectangular pulse. The pulse repetition interval (PRI) is denoted by T. The LFM for the transmit waveform has a wide sweep bandwidth and is appropriate for high-resolution sensing of the channel.

Assuming far-field point targets, the $N \times 1$ transmit steering vector is

$$\begin{aligned}\mathbf{c}(\theta) &= [c_1(\theta), \cdots, c_N(\theta)]^T \\ &= [1, e^{-j\frac{2\pi d_T}{\lambda}\theta}, \cdots, e^{-j\frac{2\pi(N-1)d_T}{\lambda}\theta}]^T,\end{aligned} \tag{4}$$

Then, the transmit signal for k-th pulse at the angular location θ is

$$\sum_{n=1}^{N-1} e^{-j\frac{2\pi n d_T}{\lambda}\theta} x_n(t - kT) \triangleq \mathbf{c}^T(\theta)\mathbf{x}(t - kT), \tag{5}$$

where $\mathbf{x}(t) = [x_1(t), \ldots, x_N(t)]^T \in \mathbb{C}^{N\times 1}$.

Assume R scatterers on the scene, each of which is characterized by the complex reflectivity $\alpha_r \in \mathbb{C}$ that is assumed constant over the array for far-field targets; time-delay $\tau_{m,n,r} \in \mathbb{R}$ corresponding to the m-th receive and n-th transmit antennas, direction-of-departure (DoD) $\theta_{n,r} = \sin\zeta_{n,r} \in \mathbb{R}$, and direction-of-arrival (DoA) $\phi_{m,r} = \sin\zeta_{m,r} \in \mathbb{R}$, where $\zeta_{n,r}$ and $\zeta_{m,r}$ are the angular locations corresponding to n-th transmit and m-th receive antenna for r-th clutter scatterer. The corresponding CCIR is

$$\begin{aligned}&h_{m,n}(\tau, \theta, \phi) \\ &\quad= \sum_{r=1}^{R} \alpha_r \delta(\tau - \tau_{m,n,r})\delta(\theta - \theta_{n,r})\delta(\phi - \phi_{m,r}).\end{aligned} \tag{6}$$

For collocated arrays, the complex reflectivity is also constant over both transmit and receive arrays, i.e., $\tau_{m,n,r} \approx \tau_r$ [48]. The delay-DoA representation of the channel is obtained by taking the Fourier transform along the spatial axes as

$$h_{m,n}(\tau, z, \tilde{z}) = \sum_{r=1}^{R} \alpha_r \delta(\tau - \tau_r) e^{-\mathrm{j}2\pi(z\theta_{n,r} + \tilde{z}\phi_{m,r})}. \tag{7}$$

The signal from each transmit antenna is reflected back by these scatterers toward a multi-antenna radar receiver. We discretize the spatial dimension in terms of ULA spacing such that the channel corresponding to the n-th transmit antenna at the location $z_n = nd_T$ and m-th receive antenna at the location $\tilde{z}_m = md_R$ is [49]

$$h_{m,n}(\tau) = \sum_{r=1}^{R} \alpha_r \delta(\tau - \tau_r) e^{-\mathrm{j}\frac{2\pi}{\lambda}(nd_T\theta_{n,r} + md_R\phi_{m,r})}. \tag{8}$$

For collocated arrays, DoD and DoA remain constant over the arrays [48]. Hence, $\theta_{n,r} \approx \theta_r$ and $\phi_{m,r} = \phi_r$. The channel is

$$\begin{aligned}h_{m,n}(\tau) &\approx h(\tau, \theta_r, \phi_r) \\ &= \sum_{r=1}^{R} \alpha_r \delta(\tau - \tau_r) e^{-\mathrm{j}\frac{2\pi}{\lambda}(nd_T\theta_r + md_R\phi_r)}.\end{aligned} \tag{9}$$

The received signal is the convolution of $h(\tau, \theta_r, \phi_r)$ with the transmit signal. Accounting for only the transmit array response vector and collecting the echoes of all transmit signals, the received signal trail at the m-th antenna for the k-th pulse is $\tilde{y}_{m,k} = \sum_{r=1}^{R} \alpha_r e^{-\mathrm{j}\frac{2\pi m d_R \phi_r}{\lambda}} \mathbf{c}^T(\theta_r)\mathbf{x}(t - kT - \tau_r)$. Denote the $M \times 1$ receive steering vector by $\mathbf{b}(\theta) = [b_1(\theta), \cdots, b_M(\theta)]^T = [1, e^{-j\frac{2\pi d_R}{\lambda}\theta}, \cdots, e^{-j\frac{2\pi(M-1)d_R}{\lambda}\theta}]^T \in \mathbb{C}^{M\times 1}$. Then, the $N \times 1$ received signal after accounting for the receive array response vector is

$$\mathbf{y}_k = \sum_{r=1}^{R} \alpha_r \mathbf{b}(\phi_r)\mathbf{c}^T(\theta_r)\mathbf{x}(t - kT - \tau_r) + \mathbf{v}_k(t), \tag{10}$$

where $\mathbf{v}_k(t)$ is the temporally and spatially additive white Gaussian noise. Again, for a collocated array, $\theta_r = \phi_r$. After filtering out signals corresponding to each transmit signal in the frequency domain at each receive antenna, define $\mathbf{a}(\theta) = f(\mathbf{b}(\theta), \mathbf{c}(\theta))$, where $f(\cdot)$ is a function of receive and transmit steering vectors. In the discretized DoA domain, wherein DoAs are aligned to a grid that matches the array resolution, Fourier beamforming produces an impulse at the scatterer location because $\mathbf{a}^H\mathbf{a} = 1$.

Hence, fixing the direction θ_r, the received signal at the m-th antenna for k-th pulse is the convolution

$$\mathbf{y}_{m,k}(t) = \sum_{n=1}^{N} (\mathbf{x}_n * \mathbf{h}_{m,n,k})(t) + \mathbf{v}_{m,k}(t),\ \forall m, \forall k. \tag{11}$$

Sampling at the Nyquist rate produces $L = BT$ samples as

$$\mathbf{y}_{m,k}[\tilde{n}] = \sum_{n=1}^{N} \sum_{l} \mathbf{x}_n[l]\mathbf{h}_{m,n,k}[\tilde{n} - l] + \mathbf{v}_{m,k}[\tilde{n}],\ \forall m, \forall k. \tag{12}$$

Further, assume $\mathbf{x}_n = [x_n[0], x_n[1], \ldots, x_n[L-1]]^T \in \mathbb{C}^{L\times 1}$ to be the discretized transmit radar signal vector of the n-th transmit antenna and $\mathbf{h}_{m,n,k} = [h_{m,n,k}[0], h_{m,n,k}[1], \ldots, h_{m,n,k}[R-1]]^T \in \mathbb{C}^{R\times 1}$ as the discretized CCIR vector corresponding to the m-th receive, n-th transmit and the k-th transmit pulse with

R range-bins. Then, the corresponding discretized received vector $\mathbf{y}_{m,k} = [\mathbf{y}_{m,1,k}, \mathbf{y}_{m,2,k}, \ldots, \mathbf{y}_{m,N,k}]^T \in \mathbb{C}^{N(L+R-1)\times 1}$ is [19, 25]

$$\mathbf{y}_{m,k} = \sum_{n=1}^{N} \mathbf{h}_{m,n,k} * \mathbf{x}_n + \mathbf{v}_{m,k}, \tag{13}$$

where the stacked noise vector $\mathbf{v}_{m,k} \in \mathbb{C}^{N(L+R-1)\times 1}$.

Rewrite (13) as

$$\mathbf{y}_{m,k} = \sum_{n=1}^{N} \mathbf{X}_n \mathbf{h}_{m,n,k} + \mathbf{v}_{m,k}, \tag{14}$$

where

$$\mathbf{X}_n = \begin{bmatrix} x_n[1] & 0 & \ldots & 0 \\ x_n[2] & x_n[1] & \ldots & 0 \\ \vdots & \vdots & \ddots & \vdots \\ x_n[L] & x_n[L-1] & \ldots & x_n[1] \\ 0 & x_n[L] & \ldots & x_n[2] \\ \vdots & \vdots & \ddots & \vdots \\ 0 & 0 & \ldots & x_n[L] \end{bmatrix} \in \mathbb{C}^{(L+R-1)\times R}, \tag{15}$$

denotes the transmit signal matrix, whose structure is determined by the LFM signal in (1). Furthermore, stacking the received vectors $\mathbf{y}_{m,k}$ for all the $1 \le m \le M$ receive antennas, one obtains

$$\mathbf{y}_k = \underbrace{(\mathbf{I}_M \otimes \mathbf{X})}_{\widetilde{\mathbf{X}} \in \mathbb{C}^{M(L+R-1)\times NMR}} \begin{bmatrix} \mathbf{h}_{1,k} \\ \mathbf{h}_{2,k} \\ \vdots \\ \mathbf{h}_{M,k} \end{bmatrix} + \begin{bmatrix} \mathbf{v}_{1,k} \\ \mathbf{v}_{2,k} \\ \vdots \\ \mathbf{v}_{M,k} \end{bmatrix},$$

$$\mathbf{y}_k = \widetilde{\mathbf{X}} \mathbf{h}_k + \mathbf{v}_k, \tag{16}$$

where $\mathbf{y}_k = \left[\mathbf{y}_{1,k}^T, \mathbf{y}_{2,k}^T, \ldots, \mathbf{y}_{M,k}^T\right]^T \in \mathbb{C}^{M(L+R-1)\times 1}$, $\mathbf{X} = [\mathbf{X}_1, \mathbf{X}_2, \ldots, \mathbf{X}_N] \in \mathbb{C}^{L+R-1\times NR}$, $\mathbf{h}_{m,k} = \left[\mathbf{h}_{m,1,k}^T, \mathbf{h}_{m,2,k}^T, \ldots, \mathbf{h}_{m,N,k}^T\right]^T \in \mathbb{C}^{NR\times 1}$, $\mathbf{h}_k = \left[\mathbf{h}_{1,k}^T, \mathbf{h}_{2,k}^T, \ldots, \mathbf{h}_{M,k}^T\right]^T \in \mathbb{C}^{NMR\times 1}$, and $\mathbf{v}_k = \left[\mathbf{v}_{1,k}^T, \mathbf{v}_{2,k}^T, \ldots, \mathbf{v}_{M,k}^T\right]^T \in \mathbb{C}^{M(L+R-1)\times 1}$. Furthermore, for the MMV scenario, we concatenate the received vector $\mathbf{y}_k$ for K subsequent pulses to obtain

$$\mathbf{Y} = [\mathbf{y}_1, \mathbf{y}_2, \ldots, \mathbf{y}_K] = \widetilde{\mathbf{X}}\mathbf{H} + \mathbf{V}, \tag{17}$$

where

$$\mathbf{H} = [\mathbf{h}_1, \mathbf{h}_2, \ldots, \mathbf{h}_K] \in \mathbb{C}^{NMR\times K}, \tag{18}$$

$$\mathbf{V} = [\mathbf{v}_1, \mathbf{v}_2, \ldots, \mathbf{v}_K] \in \mathbb{C}^{M(L+R-1)\times K}. \tag{19}$$

Since very few range bins are active or present in the entire range bin domain, each CCIR vector $\mathbf{h}_k$ is sparse in nature. Further, the sparsity profile of each $\mathbf{h}_k$ is the same, i.e., if a clutter range bin is present for the 1st pulse then it is present for all the pulses, which in turn results in the channel matrix $\mathbf{H}$ being simultaneous or row sparse in nature as shown in Fig. 1. More specifically, if the i-th row denoted as $\mathbf{H}_{i.}$ is non-zero, it implies that all the elements of the i-th row are non-zero, and vice versa. The number of pulses over which this is valid

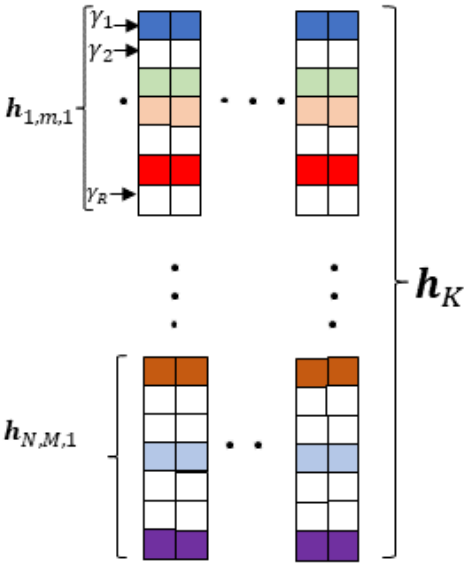

Figure 1. An illustration of simultaneously (row) sparse CCIR matrix.

depends on a number of factors including the motion of the radar platform. Finally, our goal is to estimate the simultaneously sparse CCIR matrix $\mathbf{H}$ from the multiple measurement matrix $\mathbf{Y}$. Toward this end, we employ a Bayesian learning-based framework which is described next.

III. SBL-Based Clutter CIR Estimation

Employing the SBL framework [28] on the CCIR matrix is depicted in Fig. 1, we initially assign the parameterized Gaussian prior to the i-th row of the unknown CCIR matrix $\mathbf{H}$ as

$$p\left(\mathbf{H}_{i.}, \psi_i\right) = \prod_{k=1}^{K} \left(\pi\psi_i\right)^{-1} \exp\left(-\frac{|\mathbf{H}_{i.}(k)|^2}{\psi_i}\right), \tag{20}$$

where the hyperparameter ψ_i, $1 \le i \le NMR$ denotes the prior variance corresponding to the i-th row of $\mathbf{H}$ which is unknown, and $\mathbf{\Psi} = \text{diag}\left[\psi_1, \psi_2, \ldots, \psi_{NMR}\right] \in \mathbb{R}^{NMR\times NMR}$ is the diagonal matrix of the hyperparameters. The overall PDF of the CCIR matrix is

$$p\left(\mathbf{H}, \mathbf{\Psi}\right) = \prod_{i=1}^{NMR} \prod_{k=1}^{K} \left(\pi\psi_i\right)^{-1} \exp\left(-\frac{|\mathbf{H}_{i.}(k)|^2}{\psi_i}\right). \tag{21}$$

Next, one needs to estimate the unknown hyperparameter vector $\boldsymbol{\psi}$, which can be estimated by maximizing $\log p(\mathbf{Y}; \mathbf{\Psi})$ with respect to $\boldsymbol{\psi}$, where

$$\log p(\mathbf{Y}; \mathbf{\Psi}) = \frac{-K}{2} \log |\mathbf{\Sigma}_y| - \frac{1}{2} \sum_{k=1}^{K} \mathbf{y}_k^H \mathbf{\Sigma}_y^{-1} \mathbf{y}_k. \tag{22}$$

The covariance matrix of the received vector $\mathbf{y}_k$ is $\mathbf{\Sigma}_\mathbf{y} = \left(\widetilde{\mathbf{X}}\mathbf{\Psi}\widetilde{\mathbf{X}}^H + \mathbf{R}_v\right) \in \mathbb{C}^{\tilde{M}\times\tilde{M}}$. From the above equation, it is evident that direct maximization is not possible due

to the non-convexity of the objective function. Hence, one needs to rely on the type-II evidence maximization framework which uses expectation-maximization (EM) to obtain the maximum likelihood estimate (MLE) of the hyperparameters. From the prior assignment above, as the hyperparameter $\psi_i \to 0$, the corresponding row $\mathbf{H}_i \to 0$. Consequently, the estimation of CCIR matrix $\mathbf{H}$ is transferred to the estimation of a hyperparameter vector $\boldsymbol{\psi}$ with the correct number and location of nonzero elements. Hence, the actual sparse matrix $\mathbf{H}$ acts as a latent or hidden variable and is estimated using the available observations $\mathbf{Y}$ and the hyperparameters estimated from the SBL procedure. The next subsection describes the EM algorithm used for this purpose.

A. EM Procedure

In the l-th EM iteration, let $\widehat{\boldsymbol{\Psi}}^{(l)}$ denote the estimate of the unknown hyperparameter matrix $\boldsymbol{\Psi}$.

E-Step: In this step, the average values of the latent or hidden variable are calculated given the observation matrix $\mathbf{Y}$ and the current hyperparameter estimate matrix $\widehat{\boldsymbol{\Psi}}^{(l)}$. In other words, this step helps in filling the missing data or estimating the latent variable. Toward this end, in the l-th EM iteration, the average log-likelihood $\mathcal{L}\left(\boldsymbol{\Psi}|\widehat{\boldsymbol{\Psi}}^{(l)}\right)$ of the complete data set $\{\mathbf{Y}, \mathbf{H}\}$ can be evaluated as

$$\begin{aligned}\mathcal{L}\left(\boldsymbol{\Psi}|\widehat{\boldsymbol{\Psi}}^{(l)}\right) &= \mathbb{E}_{\mathbf{H}|\mathbf{Y};\widehat{\boldsymbol{\Psi}}^{(l)}}\left\{\log p\left(\mathbf{Y},\mathbf{H};\widehat{\boldsymbol{\Psi}}^{(l)}\right)\right\} \\ &= \mathbb{E}_{\mathbf{H}|\mathbf{Y};\widehat{\boldsymbol{\Psi}}^{(l)}}\left\{\log p\left(\mathbf{Y}|\mathbf{H}\right) + \log p\left(\mathbf{H};\widehat{\boldsymbol{\Psi}}^{(l)}\right)\right\}. \quad (23)\end{aligned}$$

The first term above is

$$\begin{aligned}&\log p\left(\mathbf{Y}|\mathbf{H}\right) \\ &= -\kappa_1 - \sum_{k=1}^{K}\left(\mathbf{Y}_{.k} - \widetilde{\mathbf{X}}\mathbf{H}_{.k}\right)^H \mathbf{R}_v^{-1}\left(\mathbf{Y}_{.k} - \widetilde{\mathbf{X}}\mathbf{H}_{.k}\right),\end{aligned} \quad (24)$$

where $\kappa_1 = \log(\pi^{(N+R-1)}|\mathbf{R}_v|)$. The term above is independent of the hyperparameter covariance matrix $\boldsymbol{\Psi}^{(l)}$ and hence can be ignored in the subsequent M-Step. Furthermore, the second term in (23) reduces to

$$\begin{aligned}&\mathbb{E}_{\mathbf{H}|\mathbf{Y};\widehat{\boldsymbol{\Psi}}^{(l)}}\left\{\log p\left(\mathbf{H};\widehat{\boldsymbol{\Psi}}^{(l)}\right)\right\} \\ &= \sum_{i=1}^{NMR}\sum_{k=1}^{K} -\log\left(\pi\psi_i\right) - \frac{1}{\psi_i}\mathbb{E}_{\mathbf{H}|\mathbf{Y};\widehat{\boldsymbol{\Psi}}^{(l)}}\left\{|\mathbf{H}_{i.}(k)|^2\right\}.\end{aligned} \quad (25)$$

M-Step: In this step, the expected log-likelihood function calculated in the E-step is maximized with respect to the hyperparameters. Toward this, the objective function of the M-step can be given as

$$\widehat{\boldsymbol{\psi}}^{(l+1)} = \arg\max_{\boldsymbol{\psi}} \mathbb{E}_{\mathbf{H}|\mathbf{Y};\widehat{\boldsymbol{\Psi}}^{(l)}}\left\{\log p\left(\mathbf{H};\widehat{\boldsymbol{\Psi}}^{(l)}\right)\right\}. \quad (26)$$

In order to evaluate the above conditional expectation, one needs to evaluate the posterior PDF of $\mathbf{H}$ which is given as $p\left(\mathbf{H}|\mathbf{Y};\widehat{\boldsymbol{\Psi}}^{(l)}\right) \sim \mathcal{CN}\left(\mathcal{M}^{(l)}, \boldsymbol{\Sigma}^{(l)}\right)$, where [50]

$$\boldsymbol{\mathcal{M}}^{(l)} = \boldsymbol{\Sigma}^{(l)}\widetilde{\mathbf{X}}^H\mathbf{R}_v^{-1}\mathbf{Y} \quad (27)$$

$$\boldsymbol{\Sigma}^{(l)} = \left(\widetilde{\mathbf{X}}^H\mathbf{R}_v^{-1}\widetilde{\mathbf{X}} + \left(\widehat{\boldsymbol{\Psi}}^{(l)}\right)^{-1}\right)^{-1}, \quad (28)$$

It follows from (25) that the maximization problem is decoupled from each ψ_i. It may thus be solved to produce estimates $\widehat{\boldsymbol{\psi}}^{(l+1)}$ in the l-th EM iteration as

$$\begin{aligned}\widehat{\psi}_i^{(l+1)} &= \frac{1}{K}\sum_{k=1}^{K}\mathbb{E}_{\mathbf{H}|\mathbf{Y};\widehat{\boldsymbol{\Psi}}^{(l)}}\left\{|\mathbf{H}_{i.}(k)|^2\right\} \\ &= \boldsymbol{\Sigma}^{(l)}(i,i) + \frac{1}{K}\sum_{k=1}^{K}\left|\boldsymbol{\mathcal{M}}_{i.}^{(l)}(k)\right|^2, \forall\, i. \quad (29)\end{aligned}$$

This iterative procedure needs to be repeated till either convergence is achieved or the maximum number of EM iterations denoted by $l_{\max}$ have reached. Upon convergence, the SBL-based estimate of the sparse CCIR channel $\mathbf{H}$ is given by $\widehat{\mathbf{H}} = \boldsymbol{\mathcal{M}}^{(l)}$. This is the standard SBL procedure to estimate the simultaneously sparse channel matrix $\mathbf{H}$ for the considered MMV scenario [29]. However, this leads to a very high computational complexity of the order of $\mathcal{O}\left(N^3M^3R^3\right)$ which is a result of a need to invert a NMR dimensional matrix in the E-step. In this regard, a low complexity version of the SBL algorithm which was recently developed in [42] for the single measurement vector scenario known as covariance-free EM (CoFEM) can be invoked. In this work, we extend the CoFEM algorithm for the MMV scenario. In addition, we also take more advanced and practical scenarios of group, joint, and joint-cum-group sparse CCIR matrix estimation for the problem under consideration, which is described next.

IV. Covariance-Free SBL

One can accelerate EM procedure by avoiding the inversion of the covariance matrix given in (28). Also, by using an alternate way to calculate the diagonal elements of $\boldsymbol{\Sigma}$ which are required in the hyperparameter estimation (29). This was achieved in [42] for the SMV scenario using some linear algebra and is described next for the MMV scenario as opposed to the SMV scenario in [42]. The posterior mean matrix equation in (27) can also be equivalently written as

$$\left(\boldsymbol{\Sigma}^{(l)}\right)^{-1}\mathcal{M}^{(l)} = \widetilde{\mathbf{X}}\mathbf{R}_v^{-1}\mathbf{Y}. \quad (30)$$

Thus k-th column denoted by $\mathcal{M}_{.k}^{(l)}$ can be seen as the solution of linear system of equations $\mathbf{Cd} = \mathbf{z}$, where $\mathbf{C} = \left(\boldsymbol{\Sigma}^{(l)}\right)^{-1}$, $\mathbf{d} = \mathcal{M}_{.k}^{(l)}$ and $\mathbf{z} = \widetilde{\mathbf{X}}\mathbf{R}_v^{-1}\mathbf{Y}_{.k}$. It can be solved by the system of linear equations using conjugate gradient (CG)-algorithm [44]. Furthermore, one can find the diagonal elements of $\boldsymbol{\Sigma}^{(l)}$ employing the procedure procedure proposed in [43], which are required in M-step. We summarize the diagonal estimation procedure in the next subsection.

A. Diagonal Estimation Rule

For a square matrix $\mathbf{S} \in \mathbb{C}^{q\times q}$, an unbiased estimator of the diagonal elements, which is denoted by $\mathbf{e}$ can be evaluated using

$$\mathbf{e} = \left(\sum_{\tilde{l}=1}^{\tilde{L}} \mathbf{u}_{\tilde{l}} \odot \mathbf{w}_{\tilde{l}}\right) \oslash \left(\sum_{\tilde{l}=1}^{\tilde{L}} \mathbf{u}_{\tilde{l}} \odot \mathbf{u}_{\tilde{l}}\right), \tag{31}$$

where $\mathbf{w}_{\tilde{l}} = \mathbf{S}\mathbf{u}_{\tilde{l}}$, while $\mathbf{u}_1, \mathbf{u}_2, \ldots, \mathbf{u}_{\tilde{L}} \in \mathbb{R}^{q\times 1}$ denote $\tilde{L}$ probing vectors, consisting of independent and identically distributed (i.i.d.) elements, and satisfying $\mathbb{E}[\mathbf{u}_j(a)] = 0$ for $a = 1, \ldots, q$. The probing vectors $\mathbf{u}_{\tilde{l}}$ for $l = 1, 2, \ldots, \tilde{L}$ can be generated using Rademacher distribution which in turn implies that each element of the $\mathbf{u}_{\tilde{l}}$ will be either $+1$ or -1 with equal probability. Then, each element $\mathbf{e}(j)$ is an unbiased estimator of $\mathbf{S}(j,j)$ and $\mathbf{E}[\mathbf{e}(j)] = \mathbf{S}(j,j)$.

Hence, one can write the diagonal estimation rule in a compact form as

$$\mathbf{e} = \frac{1}{\tilde{L}} \sum_{i=1}^{\tilde{L}} \mathbf{u}_{\tilde{l}} \odot \mathbf{w}_{\tilde{l}}. \tag{32}$$

In order to utilize this rule to estimate the diagonal elements of $\mathbf{\Sigma}^{(l)}$, one needs to multiply $\mathbf{\Sigma}^{(l)}$ to each vector $\mathbf{u}_{\tilde{l}}$ to obtain $\mathbf{w}_{\tilde{l}}$; this can be done once again by solving a linear system $\left(\mathbf{\Sigma}^{(l)}\right)^{-1}\mathbf{w}_{\tilde{l}} = \mathbf{z}_{\tilde{l}}$, where $\mathbf{z}_{\tilde{l}} := \mathbf{u}_{\tilde{l}}$. Upon solving these $L+K$ parallel linear system of equations one can obtain the matrix $\mathcal{M}$ and diagonal elements $\mathbf{\Sigma}(j,j)$, for all j with lower computational complexity to simplify the computationally heavy E-step. Another interesting observation is that one can obtain the posterior mean matrix $\mathcal{M}^{(\mathbf{l})}$ and $\mathbf{w}_{\tilde{l}}$ by employing CG-algorithm to solve the linear system of equations given as $\mathbf{CW} = \mathbf{Z}$, where matrices $\mathbf{C} \in \mathbb{C}^{(L+R-1)M\times K}$ and $\mathbf{Z} \in \mathbb{C}^{(L+R-1)M\times(\tilde{L}+K)}$ are defined as follows:

$$\mathbf{C} := \left(\mathbf{\Sigma}^{(l)}\right)^{-1} = \left(\widetilde{\mathbf{X}}^H \mathbf{R}_v^{-1} \widetilde{\mathbf{X}} + \left(\mathbf{\Psi}^{(l)}\right)^{-1}\right), \tag{33}$$

$$\mathbf{Z} := \left[\boldsymbol{u}_1 \mid \boldsymbol{u}_2 \mid \ldots \mid \boldsymbol{u}_{\tilde{L}} \mid \widetilde{\mathbf{X}}^H \mathbf{R}_v^{-1} \boldsymbol{Y}\right]. \tag{34}$$

Once, we obtain the knowledge of $\boldsymbol{\mathcal{M}}^{(l)}$ and diagonal elements of $\mathbf{\Sigma}^{(l)}$, one can implement Eq.(29) to obtain the estimates of the hyperparameter vector $\boldsymbol{\psi}$. It has only a complexity of $\mathcal{O}\left(V\tilde{L}\tau\right)$, where V represents the number CG-steps required to solve linear system of equations, $\tilde{L}$ represents the number of probe vectors and τ represents the time required to calculate $\sigma_v^{-2}\widetilde{\mathbf{X}}^H\widetilde{\mathbf{X}}$ which is $\mathcal{O}\left(NMR\log(NMR)\right)$. Algorithm 1 summarizes the proposed CoFBL simultaneously sparse CCIR matrix estimation algorithm for the MMV scenario.

Algorithm 1 Covariance-free SBL-based sparse CCIR estimation

Input: $\mathbf{Y}, \widetilde{\mathbf{X}}$, ϵ (Threshold), $l_{\max}$
Output: $\widehat{\mathbf{H}}$
set $l = 1$ and $\widehat{\mathbf{\Psi}}^{(0)} = \mathbf{I}$
E-step: Compute $\mathbf{C}$ using (33)
Draw $\mathbf{u}_1$, $\mathbf{u}_2$,...,$\mathbf{u}_{\tilde{L}}$ using Rademacher distribution
Compute $\mathbf{Z}$ using (34)
$[\mathbf{w}_1|\mathbf{w}_2|\ldots|\mathbf{w}_{\tilde{L}}|\boldsymbol{\mathcal{M}}] = \mathrm{CG}(\mathbf{C}, \mathbf{Z})$
Compute $\mathbf{e}$ using (32)
M-Step: Compute $\widehat{\psi}_i^{(l+1)}$ using (29), $\forall\, i$
if $||\hat{\boldsymbol{\psi}}^{(l+1)} - \hat{\boldsymbol{\psi}}^{(l)}|| \geq \epsilon$ or $l \leq l_{\max}$
Exit
end
return $\widehat{\mathbf{H}} = \boldsymbol{\mathcal{M}}^{(l+1)}$.

If a particular range bin continues to be populated over a certain number of pulses (stationarity) and across transmit-receive antenna pairs (co-located). Further, the channel vector for the k-th pulse, $\mathbf{h}_k \in \mathbb{C}^{NMR\times 1}$, considered in this paper is obtained by stacking across the transmit antennas and followed by the receive antennas. Thus, coupled with the aforementioned fact renders structure to the sparsity, which we have attempted to exploit in Section-V. We describe three important scenarios where the simultaneously sparse CCIR matrix exhibits group, joint, and joint-cum-group sparse structure, respectively, which can be exploited further to reduce the number of hyperparameter to estimate significantly.

V. Diverse Sparsity Scenarios

The clutter patch comprising of multiple range bins and its echoes are collected over multiple pulses. This gives rise to a variety of sparse clutter scenarios encountered in practice. In the sequel, we discuss these models.

A. Group Sparsity

The parameterized Gaussian prior of the i-th group of the unknown CCIR matrix $\mathbf{H}$ as

$$p\left(\mathbf{H}_{i.}, \bar{\psi}_i\right) = \prod_{k=1}^{K} \left(\pi\bar{\psi}_i\right)^{-d} \exp\left(-\frac{\sum_{(i-1)d+1}^{id} |\mathbf{H}_{i.}(k)|^2}{\bar{\psi}_i}\right), \tag{35}$$

where d is the group sparsity cluster length, the hyperparameter $\bar{\psi}_i$, $1 \leq i \leq NMR/d$ denotes the prior variance corresponding to the i-th group of $\mathbf{H}$ which is unknown, i-th group contains indices from $(i-1)d+1$-th row to id-th row, and $\bar{\mathbf{\Psi}} = \mathrm{diag}\left[\bar{\psi}_1, \bar{\psi}_2, \ldots, \bar{\psi}_{NMR/d}\right] \in \mathbb{R}^{NMR/d\times NMR/d}$ is the diagonal matrix of the hyperparameters. The CCIR matrix is depicted in Fig. 2. The

overall PDF of the CCIR matrix is

$$p\left(\mathbf{H},\boldsymbol{\Psi}_G\right) = \prod_{i=1}^{NMR/d}\prod_{k=1}^{K}\left(\pi\bar{\psi}_i\right)^{-d}\exp\left(-\frac{\sum_{(i-1)d+1}^{id}|\mathbf{H}_{i.}(k)|^2}{\bar{\psi}_i}\right), \tag{36}$$

The hyperparameter covariance matrix $\boldsymbol{\Psi}_G$ for this scenario is given as

$$\boldsymbol{\Psi}_G = \bar{\boldsymbol{\Psi}}\otimes\mathbf{I}_d \in \mathbb{C}^{NMR\times NMR} \tag{37}$$

Theorem 1 summarizes the hyperparameter estimate for this scenario.

THEOREM 1 *In the l-th EM iteration, given $\hat{\bar{\psi}}_i^{(l-1)}$, $1\leq i\leq NMR/d$, the current hyperparameter estimates $\hat{\bar{\psi}}_i^{(l)}$ which maximizes $\mathbb{E}_{\mathbf{H}|\mathbf{Y};\widehat{\boldsymbol{\Psi}}_G^{(l)}}\left\{\log p\left(\mathbf{Y},\mathbf{H};\widehat{\boldsymbol{\Psi}}_G^{(l)}\right)\right\}$ can be evaluated as*

$$\hat{\bar{\psi}}_i^{(l)} = \frac{1}{dK}\sum_{k=1}^{K}|\mathcal{M}_G^{(l)}(\tilde{m},k)|^2 + \frac{1}{d}\boldsymbol{\Sigma}_G^{(l)}(\tilde{m},\tilde{m}), \tag{38}$$

where $\tilde{m}=(i-1)d:id$, $\boldsymbol{\mathcal{M}}_G^{(l)} = \left(\boldsymbol{\Sigma}_G^{(l)}\right)^{-1}\widetilde{\mathbf{X}}^H\mathbf{R}_v^{-1}\mathbf{Y}\in\mathbb{C}^{NMR\times K}$, $\boldsymbol{\Sigma}_G^{(l)} = \left(\widetilde{\mathbf{X}}\mathbf{R}_v^{-1}\widetilde{\mathbf{X}}^H + \left(\widehat{\boldsymbol{\Psi}}_G^{(l)}\right)^{-1}\right)^{-1}\in\mathbb{C}^{NMR\times NMR}$ are the posterior mean and covariance matrices, respectively.

Proof:
The detailed derivation is given in Appendix A. ∎

This algorithm reduces the total number of hyperparameters to be estimated by a factor of d as compared to the CoFBL algorithm. The subsequent subsection examines the situation in which the CCIR matrix has a joint sparse structure, where the channel vector $\mathbf{h}_{n,m,k}$ exhibits the same sparsity structure for each n, m and k.

B. Joint Sparsity

As depicted in Fig. 2, assuming the hyperparameter $\tilde{\psi}_i$ represents the sparsity of the i-th range bin of each channel vector $\mathbf{h}_{n,m,k}$ for all n, m and k. Hence, the prior PDF corresponding to each channel vector $\mathbf{h}_{n,m,k}$ is

$$p\left(\mathbf{h}_{n,m,k},\tilde{\boldsymbol{\psi}}\right) = \prod_{i=1}^{R}\left(\pi\tilde{\psi}_i\right)^{-1}\exp\left(-\frac{|\mathbf{h}_{n,m,k}(i)|^2}{\tilde{\psi}_i}\right), \tag{39}$$

where $\tilde{\boldsymbol{\psi}} = [\tilde{\psi}_1,\tilde{\psi}_2,\ldots,\tilde{\psi}_R]^T\in\mathbb{R}^{R\times 1}$ and $\widetilde{\boldsymbol{\Psi}} = \text{diag}\left[\tilde{\boldsymbol{\psi}}\right]\in\mathbb{R}^{R\times R}$. Let the hyperparameter covariance matrix for this scenario is

$$\boldsymbol{\Psi}_J = \left(\mathbf{I}_M\otimes\left(\mathbf{I}_N\otimes\widetilde{\boldsymbol{\Psi}}\right)\right)\in\mathbb{C}^{NMR\times NMR} \tag{40}$$

Hence, the prior PDF of the channel matrix $\mathbf{H}$ is

$$p\left(\mathbf{H},\boldsymbol{\Psi}_J\right) = \prod_{n=1}^{N}\prod_{m=1}^{M}\prod_{k=1}^{K}\prod_{i=1}^{R}\left(\pi\tilde{\psi}_i\right)^{-1}\exp\left(-\frac{|\mathbf{h}_{n,m,k}(i)|^2}{\tilde{\psi}_i}\right), \tag{41}$$

The following theorem summarizes the hyperparameter estimates for this scenario.

THEOREM 2 *In the l-th EM iteration, given $\hat{\tilde{\psi}}_i^{(l-1)}$, $1\leq i\leq R$, the current hyperparameter estimates $\hat{\tilde{\psi}}_i^{(l)}$ which maximizes $\mathbb{E}_{\mathbf{H}|\mathbf{Y};\widehat{\boldsymbol{\Psi}}_J^{(l)}}\left\{\log p\left(\mathbf{Y},\mathbf{H};\widehat{\boldsymbol{\Psi}}_J^{(l)}\right)\right\}$ can be evaluated as*

$$\hat{\tilde{\psi}}_i^{(l)} = \frac{1}{NMK}\sum_{n=1}^{N}\sum_{m=1}^{M}\sum_{k=1}^{K}|\bar{\mathcal{M}}_J^{(l)}(\bar{m}+i,k)|^2 + \frac{1}{NM}\sum_{n=1}^{N}\sum_{m=1}^{M}\bar{\boldsymbol{\Sigma}}_J^{(l)}(\bar{m}+i,\bar{m}+i), \tag{42}$$

where $\bar{m}=(m-1)NR+(n-1)R$.

Proof:
See Appendix B. ∎

The quantities $\bar{\mathcal{M}}_J^{(l)}$ and $\bar{\boldsymbol{\Sigma}}_J^{(l)}$ represent the posterior mean and covariance matrices for the CCIR matrix $\mathbf{H}$ for the joint sparse scenario, which can be obtained from (26) and (27), respectively by replacing the hyperparameter covariance matrix $\widehat{\boldsymbol{\Psi}}$ by $\widehat{\boldsymbol{\Psi}}_J$. The detailed proof of the above theorem is given in Appendix B. Please note that in each EM iteration, the total number of hyperparameters that one needs to estimate reduces to R in contrast to the NMR for the CoFBL algorithm. This results in significant computational resource savings and makes the algorithm faster.

C. Joint-Cum-Group Sparsity

Furthermore, the clutter patches generally occur in patches and hence if a particular range bin is active then there is a very high possibility that the nearby range bins are also active in practice. This makes the unknown sparse CCIR matrix joint-cum-group sparse in nature as depicted in Fig. 2. Therefore, the parameterized Gaussian prior to the clutter channel $\mathbf{h}_{n,m,k}$ for this scenario can be assigned as

$$p(\mathbf{h}_{n,m,k};\underline{\boldsymbol{\psi}}) = \prod_{i=1}^{R/d}\frac{1}{(\pi\underline{\psi}_i)^d}\exp\left(-\frac{\sum_{(i-1)d+1}^{id}|\mathbf{h}_{n,m,k}(i)|^2}{\underline{\psi}_i}\right),$$

where d represents the group sparsity cluster length, $\underline{\boldsymbol{\psi}} = [\underline{\psi}_1,\underline{\psi}_2,\ldots,\underline{\psi}_{\frac{R}{d}}]^T\in\mathbb{R}^{\frac{R}{d}\times 1}$, and $\underline{\boldsymbol{\Psi}} = \text{diag}\left(\underline{\boldsymbol{\psi}}\right)\in\mathbb{R}^{\frac{R}{d}\times\frac{R}{d}}$. The prior corresponding to the MMV clutter channel matrix $\mathbf{H}\in\mathbb{C}^{NMR\times K}$ for this scenario is given as

$$p\left(\mathbf{H};\underline{\boldsymbol{\Psi}}_{JG}\right) = \prod_{n=1}^{N}\prod_{m=1}^{M}\prod_{k=1}^{K}\prod_{i=1}^{R/d}\frac{1}{(\pi\underline{\psi}_i)^d}\exp\left(-\frac{\sum_{(i-1)d+1}^{id}|\mathbf{h}_{n,m,k}(i)|^2}{\underline{\psi}_i}\right). \tag{43}$$

The hyperparameter covariance matrix $\boldsymbol{\Psi}_{JG}$ for this scenario is given as

$$\boldsymbol{\Psi}_{JG} = \left(\mathbf{I}_M\otimes\left(\mathbf{I}_N\otimes\left(\underline{\boldsymbol{\Psi}}\otimes\mathbf{I}_d\right)\right)\right)\in\mathbb{C}^{NMR\times NMR} \tag{44}$$

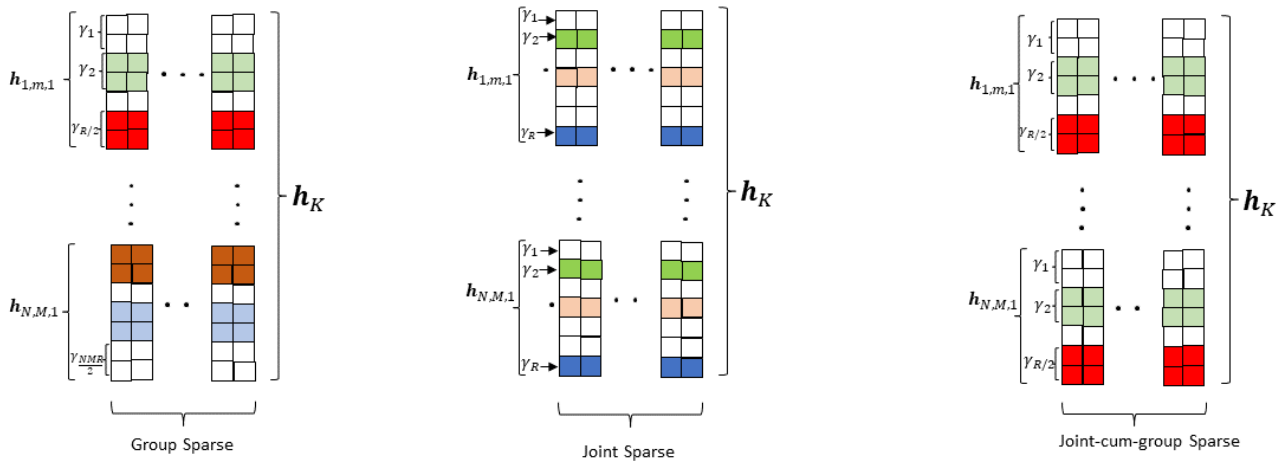

Figure 2. Illustrations of group, joint, and joint-cum-group sparse CCIR matrices.

Theorem 3 summarizes the hyperparameter estimate for this scenario.

THEOREM 3 *In the l-th EM iteration, given $\widehat{\underline{\psi}}_i^{(l-1)}$, $1 \leq i \leq R/n$, the current hyperparameter estimates $\widehat{\underline{\psi}}_i^{(l)}$ which maximizes $\mathbb{E}_{\mathbf{H}|\mathbf{Y};\widehat{\mathbf{\Psi}}^{(l)}} \left\{ \log p \left(\mathbf{Y}, \mathbf{H}; \widehat{\mathbf{\Psi}}_{JG}^{(l)} \right) \right\}$ can be evaluated as*

$$\widehat{\underline{\psi}}_i^{(l)} = \frac{1}{dNMK} \sum_{n=1}^{N} \sum_{m=1}^{M} \sum_{k=1}^{K} |\mathcal{M}_{JG}^{(l)}(\underline{m}, k)|^2 + \frac{1}{dNM} \sum_{n=1}^{N} \sum_{m=1}^{M} \mathbf{\Sigma}_{JG}^{(l)}(\underline{m}, \underline{m}), \tag{45}$$

where $\underline{m} = \bar{m} + (i-1)d : \bar{m} + id$.

Proof:
The detailed derivation is given in Appendix C. ■

In contrast to CoFBL, which estimates total NMR hyperparameters in each SBL iteration, and CoFGBL which requires to estimate $\frac{NMR}{d}$ hyperparameter in each EM iteration, and CoFJBL which requires to estimate R hyperparameter in each EM iteration, the proposed CoFJGBL requires only R/d hyperparameters to be estimated. This further reduces computational complexity and enhances the overall efficient resource utilization. Algorithm 2 summarizes the different CoFBL sparse CCIR matrix estimation algorithms for MMV scenarios. While some apriori information about the scene to be estimated would help in the selection of appropriate technique, one could undertake the following approach. A few SBL iterations using the CoFBL technique can be used initially to estimate CCIR, and based on the emergence of sparsity structure, one could use COFGBL, CoFJBL and COFGJBL techniques to leverage additional degree of freedom. The next sub-section briefly discusses the computational complexity of the proposed algorithms.

Table II
Computational complexities of the various proposed algorithms

Algorithm	Conventional EM-based SBL	Proposed methods
CoFBL	$\mathcal{O}\left(N^3M^3R^3\right)$	$\mathcal{O}\left(V_M\tilde{L}_M\tau_M\right)$
CoFGBL	$\mathcal{O}\left(N^3M^3R^3\right)$	$\mathcal{O}\left(V_G\tilde{L}_G\tau_G\right)$
CoFJBL	$\mathcal{O}\left(N^3M^3R^3\right)$	$\mathcal{O}\left(V_J\tilde{L}_J\tau_J\right)$
CoFJGBL	$\mathcal{O}\left(N^3M^3R^3\right)$	$\mathcal{O}\left(V_{JG}\tilde{L}_{JG}\tau_{JG}\right)$

D. Computational Complexity

The per EM iteration computational complexities of the various proposed scheme for the conventional SBL-based implementation is given in table II. The computational complexity reduces since the number of hyperparameters that are to be estimated in every algorithm reduces as a result of exploiting the additional structural sparsity. It can be further reduced with the covariance-free EM-based implementation, which leads to the computational complexity of the $\mathcal{O}\left(U_i\tilde{L}_i\tau_i\right)$, where U_i is the number of CGD steps, $\tilde{L}_i$ is the total number of probe vectors and τ_i is the complexity of the matrix multiplication $\widetilde{\mathbf{X}}\widetilde{\mathbf{X}}^H$ in each of the proposed algorithm, where $i \in \{M, G, J, JG\}$ represents the different algorithms. Utilizing the interpretable nature and computational efficiency of CoFBL, CoFAR systems achieve accurate clutter CIR estimation while ensuring transparency in the underlying processes, unlike deep learning methods. This supports CoFAR's goal of conserving resources for environment knowledge acquisition while prioritizing radar surveillance tasks.

The primary goal of the CoFBL algorithm is to reduce computational complexity when estimating large-dimensional sparse quantities [42]. If the sparse quantity is not sufficiently large, the computational advantage of CoFBL will be minimal. Moreover, the computational complexity of the CoFBL algorithm is influenced by the number of conjugate gradient steps needed to solve the linear system of equations. Therefore, if the condition

Algorithm 2 Covariance-free SBL-based joint, group, and joint-cum-group sparse CCIR estimation

Input: $\mathbf{Y}, \widetilde{\mathbf{X}}$, ϵ (Threshold), $l_{\max}$
Output: $\widehat{\mathbf{H}}$
Group Sparse
set $l=1$ and $\widehat{\mathbf{\Psi}}_G^{(0)}=\mathbf{I}$
for $||\hat{\bar{\boldsymbol{\psi}}}^{(l+1)}-\hat{\bar{\boldsymbol{\psi}}}^{(l)}||\geq\epsilon$ or $l\leq l_{\max}$
E-step: Compute $\mathbf{C}=\left(\widetilde{\mathbf{X}}^H\mathbf{R}_v^{-1}\widetilde{\mathbf{X}}+\left(\widehat{\mathbf{\Psi}}_G^{(l)}\right)^{-1}\right)^{-1}$
Draw $\mathbf{u}_1$, $\mathbf{u}_2$,...,$\mathbf{u}_{\tilde{L}}$ using Rademacher distribution
Compute $\mathbf{Z}$ using (34)
$[\mathbf{w}_1,\mathbf{w}_2,\ldots,\mathbf{w}_L|\mathcal{M}]=\mathrm{CG}(\mathbf{C},\mathbf{Z})$
Compute $\mathbf{e}$ using (32)
M-Step: Compute $\widehat{\bar{\psi}}_i^{(l+1)}$ using (38), $\forall\, i$
end
return $\widehat{\mathbf{H}}=\boldsymbol{\mathcal{M}}_G^{(l+1)}$.
Joint Sparse
set $l=1$ and $\widehat{\mathbf{\Psi}}_J^{(0)}=\mathbf{I}$
for $||\hat{\bar{\boldsymbol{\psi}}}^{(l+1)}-\hat{\bar{\boldsymbol{\psi}}}^{(l)}||\geq\epsilon$ or $l\leq l_{\max}$
E-step: Compute $\mathbf{C}=\left(\widetilde{\mathbf{X}}^H\mathbf{R}_v^{-1}\widetilde{\mathbf{X}}+\left(\widehat{\widehat{\mathbf{\Psi}}}_J^{(l)}\right)^{-1}\right)^{-1}$
Draw $\mathbf{u}_1$, $\mathbf{u}_2$,...,$\mathbf{u}_{\tilde{L}}$ using Rademacher distribution
Compute $\mathbf{Z}$ using (34)
$[\mathbf{w}_1,\mathbf{w}_2,\ldots,\mathbf{w}_L|\mathcal{M}]=\mathrm{CG}(\mathbf{C},\mathbf{Z})$
Compute $\mathbf{e}$ using (32)
M-Step: Compute $\widehat{\bar{\psi}}_i^{(l+1)}$ using (42), $\forall\, i$
end
return $\widehat{\mathbf{H}}=\boldsymbol{\mathcal{M}}_J^{(l+1)}$.
Joint-Cum-Group Sparse
set $l=1$ and $\widehat{\mathbf{\Psi}}_{JG}^{(0)}=\mathbf{I}$
for $||\hat{\underline{\psi}}^{(l+1)}-\hat{\underline{\psi}}^{(l)}||\geq\epsilon$ or $l\leq l_{\max}$
E-step: Compute $\mathbf{C}=\left(\widetilde{\mathbf{X}}^H\mathbf{R}_v^{-1}\widetilde{\mathbf{X}}+\left(\widehat{\mathbf{\Psi}}_{JG}^{(l)}\right)^{-1}\right)^{-1}$
Draw $\mathbf{u}_1$, $\mathbf{u}_2$,...,$\mathbf{u}_{\tilde{L}}$ using Rademacher distribution
Compute $\mathbf{Z}$ using (34)
$[\mathbf{w}_1,\mathbf{w}_2,\ldots,\mathbf{w}_L|\mathcal{M}]=\mathrm{CG}(\mathbf{C},\mathbf{Z})$
Compute $\mathbf{e}$ using (32)
M-Step: Compute $\widehat{\underline{\psi}}_i^{(l+1)}$ using (45), $\forall\, i$
end
return $\widehat{\mathbf{H}}=\boldsymbol{\mathcal{M}}_{JG}^{(l+1)}$.

number of the matrix $\mathbf{C}=\left(\widetilde{\mathbf{X}}^H\mathbf{R}_v^{-1}\widetilde{\mathbf{X}}+\left(\mathbf{\Psi}^{(l)}\right)^{-1}\right)$ is very high, a preconditioner matrix may be necessary to accelerate the convergence of the conjugate gradient algorithm [42]. Nevertheless, the number of conjugate gradient iterations V will always be less than or equal to NMR, the length of the unknown sparse quantity [44].

VI. Bayesian Cramér-Rao Bounds (BCRBs)

In this section, we derived BCRB bound for the various algorithms proposed in this work. For any unbiased estimation technique, BCRB serves as a lower bound on the MSE.

PROPOSITION 1 *The BCRB for the CoFBL technique is*

$$\mathrm{E}\left[\left\|\widehat{\underline{\mathbf{H}}}-\underline{\mathbf{H}}\right\|_F^2\right]\geq\mathrm{Tr}\left[\left(\sigma^{-2}\left(\widetilde{\mathbf{X}}^H\widetilde{\mathbf{X}}\right)\otimes\mathbf{I}_K+\mathbf{\Psi}^{-1}\otimes\mathbf{I}_K\right)^{-1}\right]$$

Proof:
Contrary to the CRB framework, which does not take prior PDF of the unknown quantity into account, BL framework [28] assigns a parametric prior PDF in (36), and it serves a lower bound on the estimation performance of the CoFBL algorithm. Employing the BCRB framework, the total Fisher Information Matrix (FIM) $\mathbf{J}_T$ for the unknown CCIR matrix $\mathbf{H}$ is defined as $\mathbf{J}_T=\mathbf{J}_D+\mathbf{J}_P$, where $\mathbf{J}_D$ and $\mathbf{J}_P$ are the FIMs of the observed data and prior, respectively. After vectorizing Eq. (17), and defining $\bar{\mathbf{X}}=\left(\mathbf{I}_K\otimes\tilde{\mathbf{X}}\right)\in\mathbb{C}^{MK(K+R-1)\times KNMR}$, one obtains $\mathbf{y}=\bar{\mathbf{X}}\mathbf{h}+\bar{\mathbf{v}}$. Hence, $\mathbf{J}_T$ can be mathematically represented as

$$\mathbf{J}_T=\underbrace{-\mathrm{E}_{(\underline{\mathbf{y}},\underline{\mathbf{h}})}\left[\frac{\partial^2\mathcal{L}\left(\underline{\mathbf{y}}|\underline{\mathbf{h}};\mathbf{P}\right)}{\partial\underline{\mathbf{h}}\partial\underline{\mathbf{h}}^H}\right]}_{\mathbf{J}_D}\underbrace{-\mathrm{E}_{\underline{\mathbf{h}}}\left[\frac{\partial^2\mathcal{L}\left(\underline{\mathbf{h}};\mathbf{P}\right)}{\partial\underline{\mathbf{h}}\partial\underline{\mathbf{h}}^H}\right]}_{\mathbf{J}_P},\tag{46}$$

where $\mathbf{y}=\mathrm{vec}\left(\mathbf{Y}\right)\in\mathbb{C}^{K(K+R-1)\times1}$ and $\mathbf{h}=\mathrm{vec}\left(\mathbf{H}\right)\in\mathbb{C}^{KNMR\times1}$, and $\mathbf{P}=\mathbb{E}[\mathbf{h}\mathbf{h}^H]\in\mathbb{C}^{KNMR\times KNMR}$. The log-likelihoods of the observation vector $\mathbf{y}$ and CCIR vector $\mathbf{h}$ are defined as $\mathcal{L}\left(\underline{\mathbf{y}}|\underline{\mathbf{h}};\mathbf{P}\right)=\log p(\underline{\mathbf{y}}|\underline{\mathbf{h}};\mathbf{P})$ and $\mathcal{L}\left(\underline{\mathbf{h}};\mathbf{P}\right)=\log\left(\underline{\mathbf{h}};\mathbf{P}\right)$, respectively, which are parameterized by $\mathbf{P}$. Using (21), the log-likelihood is given as

$$\mathcal{L}\left(\underline{\mathbf{h}};\mathbf{P}\right)=\left(c-\underline{\mathbf{h}}^H\mathbf{P}^{-1}\underline{\mathbf{h}}\right),$$

where $c=-NMK\log(\pi)-\log(|\mathbf{P}|)$, which yields

$$\mathbf{J}_P=\mathrm{E}_{\underline{\mathbf{h}}}\left[\frac{\partial^2\mathcal{L}\left(\underline{\mathbf{h}};\mathbf{P}\right)}{\partial\underline{\mathbf{h}}\partial\underline{\mathbf{h}}^H}\right]=\mathbf{P}^{-1}.$$

Using $\mathcal{L}\left(\underline{\mathbf{y}}|\underline{\mathbf{h}};\mathbf{P}\right)=\frac{1}{\sigma_v^2}||\mathbf{y}-\widetilde{\mathbf{X}}\mathbf{h}||^2$, the $\mathbf{J}_D$ is

$$\mathbf{J}_D=\mathrm{E}_{(\underline{\mathbf{y}},\underline{\mathbf{h}})}\left[\frac{\partial^2\mathcal{L}\left(\underline{\mathbf{y}}|\underline{\mathbf{h}};\mathbf{P}\right)}{\partial\underline{\mathbf{h}}\partial\underline{\mathbf{h}}^H}\right]=\sigma^{-2}\bar{\mathbf{X}}^H\bar{\mathbf{X}},$$

with the BCRB given by

$$\mathbf{J}_B^{-1}=\left(\sigma^{-2}\widetilde{\mathbf{X}}^H\widetilde{\mathbf{X}}+\mathbf{P}^{-1}\right)^{-1}.$$

After substituting $\mathbf{P}=\mathbf{\Psi}\otimes\mathbf{I}_K$ in the above equation, the BCRB bound for $\widehat{\mathbf{H}}$ is obtained as

$$\mathrm{E}\left[\left\|\widehat{\underline{\mathbf{H}}}-\underline{\mathbf{H}}\right\|_F^2\right]\geq\mathrm{Tr}\left[\left(\sigma^{-2}\left(\widetilde{\mathbf{X}}^H\widetilde{\mathbf{X}}\right)\otimes\mathbf{I}_K+\mathbf{\Psi}^{-1}\otimes\mathbf{I}_K\right)^{-1}\right].$$

■

In order to derive the BCRBs for the scenarios with group, joint, and joint-cum-group sparse CCIR matrix estimation one can replace the hyperparameter covariance matrix $\mathbf{\Psi}$ above by the corresponding hyperparameter covariance matrix in the above expression. Next, in order to show the efficacy of the proposed algorithm we have carried out comprehensive simulations on the simulated as well as practical CCIR obtained by RFView®.

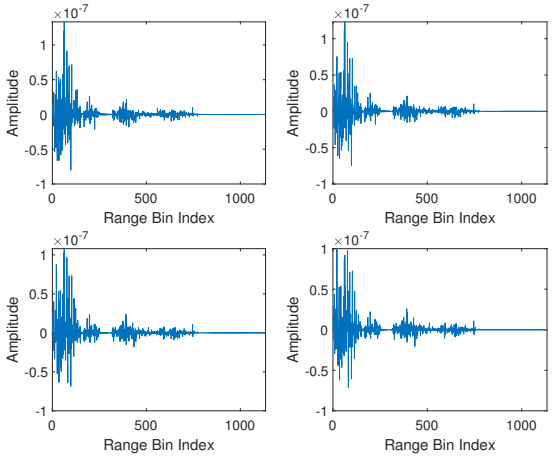

Figure 3. Different channels obtained from RFview depicting the sparsity in the range bin domain.

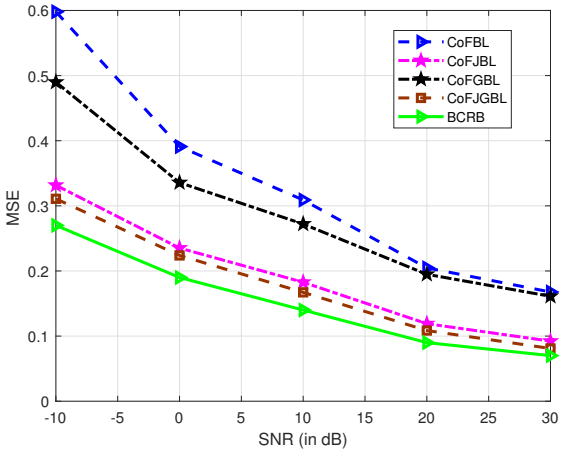

Figure 4. MSE versus SNR for the proposed sparse CCIR estimation algorithms.

VII. Numerical Experiments

We assessed the efficacy of the covariance-free Bayesian learning techniques for simultaneous, joint, and joint-cum-group sparse MIMO clutter CIR estimation using synthetic data generated from RFView® [51], an advanced modeling and simulation software. The RFView® Modeling & Simulation tool, developed by Information Systems Laboratories, Inc. (ISL), is an advanced, site-specific RF simulation and analysis tool. It offers highly precise characterization of complex RF environments, making it ideal for system analysis, test planning, generating high-fidelity synthetic data, and developing signal processing algorithms [25, 51]. RFView® intelligently divides the clutter region into separate patches based on publicly available topographical data and land cover classifications to accurately model ground clutter returns for radio frequency systems. The dataset produced by RFView® represents a monostatic radar platform moving at a velocity of 100 m/s across Southern California. In our evaluation, we considered a MIMO scenario featuring $N = 3$ transmitters and $M = 2$ receivers. Each transmitter emitted $K = 64$ pulses of a Linear Frequency Modulated (LFM) waveforms with a bandwidth of 100, 200 and 300 KHz, respectively, and all of them have pulse repetition frequency of 1 KHz. The CCIR generated by RFView® has dimensions $3\times2\times64\times1134$, where $R = 1134$ denotes the number of range bins.

Fig. 4 depicts the MSE performance of the various proposed MSBL-based sparse CCIR estimation methods as a function of signal-to-noise ratio (SNR). As expected, with increasing SNR, the MSE tends to decrease for all the proposed algorithms because, with an increment in SNR, the distortion due to noise tends to decrease, which results in improved estimation performance. It is also evident from the figure that joint, group, and joint-cum-group BL algorithms not only reduce the number of hyperparameters but also yield better MSE performance

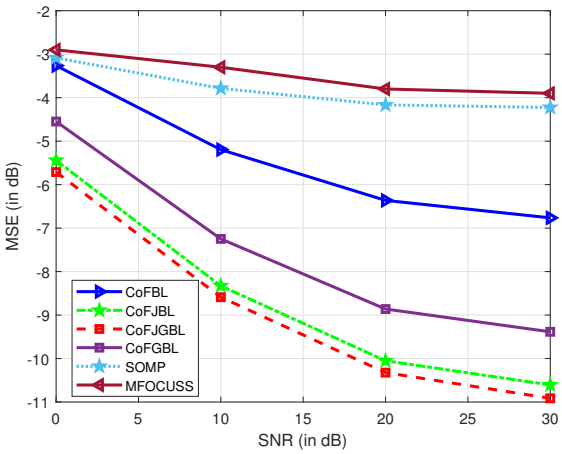

Figure 5. MSE versus SNR performance comparison for the proposed algorithms and the SOMP and MFOCUSS algorithms.

in comparison to the CoFBL algorithm in the same order as mentioned above. This is happening because we are able to exploit the sparsity structure efficiently.

Fig. 5 demonstrates the performance comparison with other existing simultaneous sparse signal estimation methods in the literature namely simultaneous orthogonal matching pursuit (SOMP) [52] and *m*ultiple *foc*al *u*nderdetermined *s*ystem *s*olver (MFOCUSS) [53]. Herein, the considered algorithms solve equation (14) and their respective MSEs are plotted. It can be readily seen that the proposed Bayesian learning algorithm outperforms the SOMP and MFOCUSS algorithms which are sensitive to the dictionary matrix and require prior information about the sparsity level. The poor performance of the SOMP can be attributed to its sensitivity to the stopping parameter as well as to the sensing matrix $\widetilde{\mathbf{X}}$ [54], while the poor performance of the MFOCUSS arises due to its convergence deficiencies and sensitivity to the

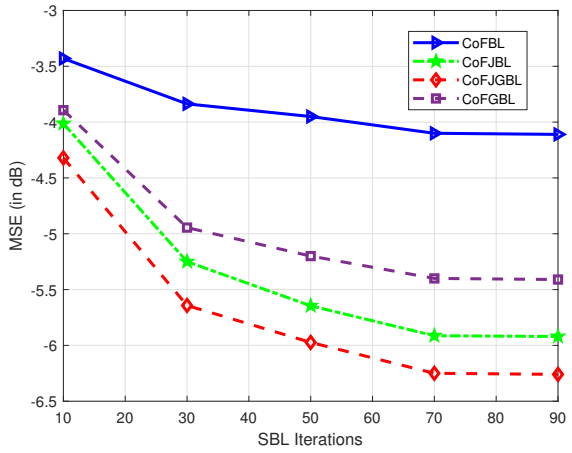

Figure 6. MSE versus EM iterations for the proposed algorithms.

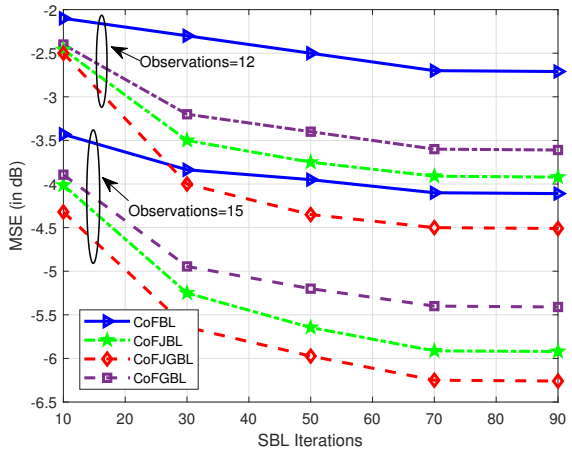

Figure 7. MSE versus EM iterations for the proposed algorithms for different observations.

regularization parameter [55]. By contrast, the proposed CoFBL-based design is robust to the sensing matrix $\widetilde{\mathbf{X}}$, and the well-established properties of its cost-function of (19), as described in [28, 29], followed by the EM-framework, guarantees convergence to sparse solutions.

Next, two plots are derived for the simulated data. Fig. 6 plots MSE as a function of a number of EM iterations. As the number of EM iterations increases the hyperparameters are achieving convergence and the proposed design is able to capture the sparsity in a better way. Fig. 7 plots the MSE as a function of SBL or EM iterations for the different number of measurements at the receiver. It can be readily observed from the figure as we reduce the number of observations the MSE performance deteriorates because there is very little information available for the underlying quantity to be estimated.

Table-III demonstrates the accuracy and efficiency as the normalized MSE (in percentage) and Python run time (in seconds), respectively. We have used Intel core i9 2.5 GHz processor 32 GB RAM to carry out this numerical analysis. It has been observed that the proposed CoFBL algorithm has better estimation accuracy and also a very efficient run-time. This shows the effectiveness of the proposed algorithm.

Fig. 8 showcases the MSE performance of the CoFGBL algorithm in different scenarios, considering the SNR as a variable. The first scenario explores the case where the underlying CCIR adheres to the group sparsity assumption. In the second and third scenarios, a model mismatch of 5% and 10% is introduced, respectively. As anticipated, when the actual sparsity deviates from the group sparsity assumption, the MSE performance of the CoFGBL algorithm is adversely affected, resulting in a higher MSE compared to the ideal scenario that conforms to the group sparse structure. At low SNR levels, the impact on MSE is not significant due to the dominant effect of noise. However, as the SNR increases, the difference in MSE becomes more noticeable, with the magnitude of mismatch directly influencing the observed increase.

Further, we demonstrate the effect of model mismatch on CoFAR's target detection performance. We considered a scenario for a target moving with a Doppler velocity of 100 km/h. The received signal is

$$\mathbf{y} = \mathbf{H}_c\mathbf{x} + \mathbf{H}_t\left(\mathbf{x} \odot \mathbf{p}\right) + \mathbf{n}, \tag{47}$$

where $\mathbf{H}_c$, $\mathbf{H}_t$, $\mathbf{x}$, $\mathbf{p}$, and $\mathbf{n}$ represent the convolution CCIR matrix, convolution target matrix, transmit waveform vector, Doppler vector, and receive noise vector, respectively. After estimating CCIR using the proposed CoFGBL algorithm, we evaluate the minimum variance distortionless response (MVDR) beamformer [56] of the clutter channel for three scenarios: true CCIR (clairvoyant), CoFGBL-estimated CCIR with known model (estimated CoFGBL), and CoFGBL-estimated CCIR with model mismatch, respectively. Two model mismatch scenarios are considered, wherein 5 and 10 percent additional non-zero elements are added at random locations that were not included in the group sparse structure. For each of these MVDR beamformers, we evaluate the respective signal-to-clutter-plus-noise ratio (SCNR). It follows from Fig. 9 that the SCNR performance of estimated CoFGBL algorithm is closest to the clairvoyant case, while the scenarios with model mismatch results in SCNR loss. For instance, at SNR $= 10$ dB, the SCNR degrades by ≈ 1 and ≈ 2 dB below estimated CoFGBL performance for 5 and 10 percent mismatch, respectively.

Fig. 10 shows the MSE performance of the proposed CoFBL technique for the different number for different receive antennas while the transmit antennas are set equal to 4 and 8. Since, increasing the number of antennas will increase the dimension of the unknown sparse CCIR vector $\mathbf{h}_k \in \mathbb{C}^{NMR}$, where N, M, and R represents the number of transmit antennas, receive antennas, and range bins, respectively. Hence the MSE increases but as it can be seen in the figure that it is not a substantial increment. Hence, one can conclude that the estimation

Table III
Accuracy versus efficiency trade off between the conventional EM and proposed CoFBL algorithms

EM-iteration	Conventional SBL		CoFBL	
	Accuracy (%)	Run Time (Seconds)	Accuracy (%)	Run Time (Seconds)
10	51.58	3.91	50.26	1.4
20	21.05	7.31	16.96	2.21
30	4.38	11.42	3.65	3.05
40	3.29	15.89	3.20	4.10
50	2.94	19.65	2.91	5.04

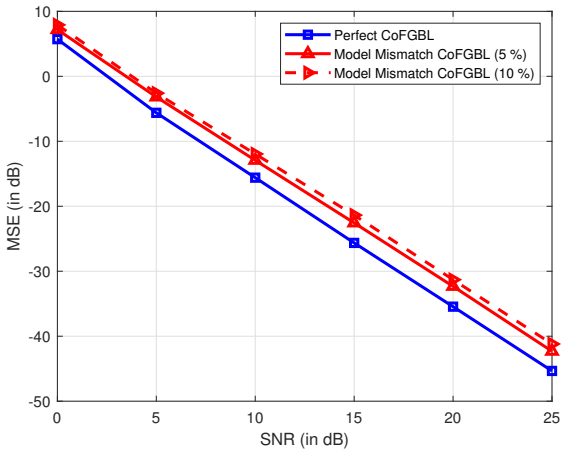

Figure 8. Model mismatch analysis

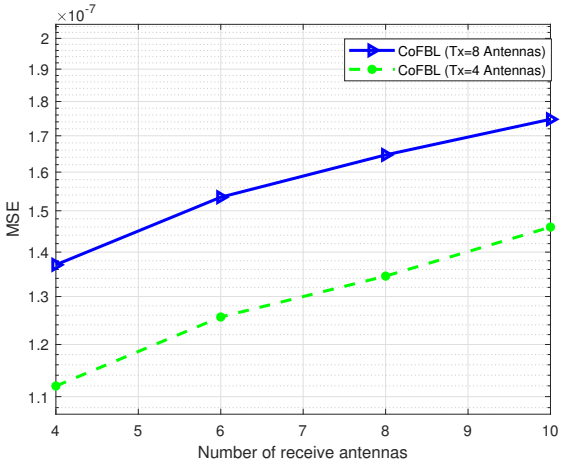

Figure 10. MSE as function of receive antennas.

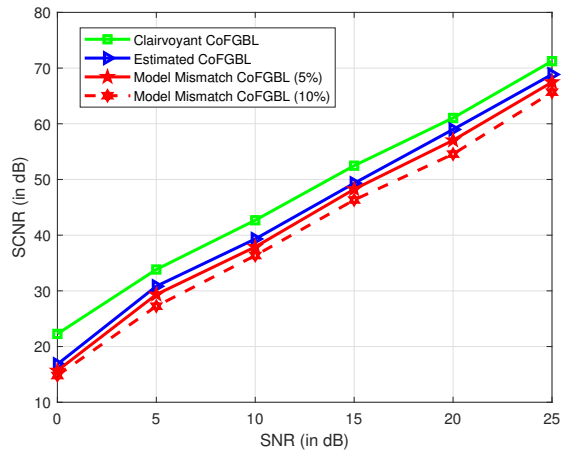

Figure 9. SCNR analysis for the CoFGBL algorithm in model mismatch scenario with MVDR.

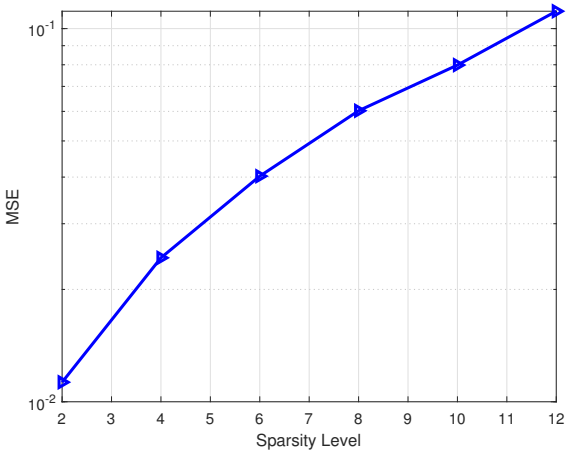

Figure 11. MSE as a function of sparsity level.

performance is not getting affected much with the increase in number of transmit and receive antennas. On the other hand, this would increase the computation complexity of conventional SBL algorithm, i.e.. $\mathcal{O}\left(N^3M^3R^3\right)$. While, the computational complexity of CoFBL algorithm is $\mathcal{O}\left(UL\tau\right)$, which is linear in terms of N and M. Hence, for a practical MIMO radar with more number of transmit and receive antennas the CoFBL becomes more computationally effective.

Fig. 11 demonstrates the MSE of the CoFBL algorithms as a function of sparsity level of the sparse CCIR matrix, i.e., the number of non-zero rows. It can be readily observed that as the number of non-zero rows increases the MSE increases since, the number of elements which are to be estimated also increases and hence the estimation error increases. Fig. 12 depicts MSE performance of the CoFGBL algorithm for the different cluster lengths as a funtion of SNR. As it can be readily seen in the figure that with increasing cluster length one will have the lower

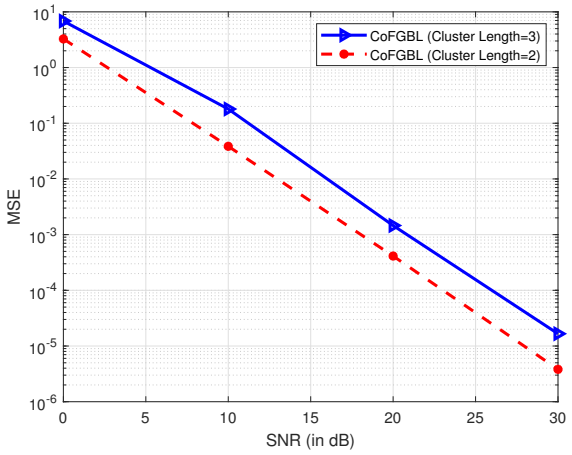

Figure 12. MSE versus SNR for CoFGBL with different cluster length

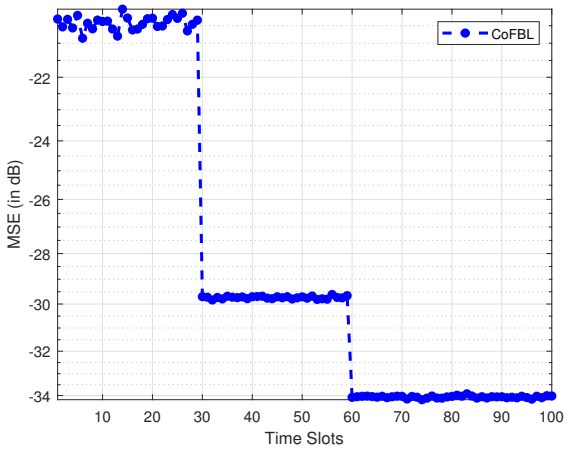

Figure 13. CoFBL performance performance with changing environment.

computational complexity but it comes at the cost of increased MSE.

Fig. 13 illustrates the MSE performance of the proposed CoFBL algorithm in a dynamic environment. It depicts the algorithm's ability to adapt to changing conditions over time. In this simulation, the sparsity profile remains constant for the initial 30 time slots. From the 31st to the 60th time slot, there is a 10 percent decrease in the sparsity profile, followed by an additional 10 percent decrement from the 60th to the 100th time slot. This clearly demonstrates that the CoFBL algorithm successfully tracks the changing environment. As the number of elements to be estimated decreases, there is a corresponding reduction in the MSE.

VIII. Summary

In this paper, we analyzed the MIMO CCIR estimation problem in CoFAR. We devised different covariance-free BL-based CCIR estimation approaches that leverage the simultaneous, joint, and joint-cum-group sparsity of the CCIR. The numerical results imply that the suggested BL-based CCIR estimation strategy outperforms the other sparse estimation techniques such as SOMP and MFOCUSS while using fewer resources such as pilot length. This implies that using the proposed algorithms one can save critical resources like time and power, which can be further utilized for the primary function of target detection in CoFAR.

In the future, the proposed CoFBL technique and its variants show potential for utilization in conventional radar applications such as target imaging and parameter estimation [32, 57]. These applications are characterized by scenarios where only a few targets are present, creating an ideal condition that can be modeled as a sparse recovery problem. Additionally, the integration of sensing and communication is an emerging research area for 6G wireless systems [58–60], where both radar and communication systems operate in the same frequency band. 6G technologies, including terahertz/millimeter-wave (mmWave) and orthogonal time-frequency space (OTFS), exhibit sparsity in the wireless channels. When combined with radar systems that encounter only a limited number of targets or clutter patches, the problem can once again be formulated as a sparse recovery problem that can be effectively addressed using the CoFBL technique.

Sea clutter [61, 62] presents unique modeling complexities due to its non-stationary nature. Accurately representing it with the models considered in this paper requires thorough investigation. Preliminary work in this area can be found in [25]. While the current models can handle non-stationary scenarios using the single measurement vector setup, applying this approach to sea clutter remains a topic for future research.

The CoFBL technique holds promise for various research problems, including joint CCIR estimation and waveform design, and it would be interesting to extend it to scenarios where the underlying sparse CCIR vectors exhibit correlation [23]. Apart from radar applications, the CoFBL and its variants find utility in estimating sparse wireless channels in mmWave [63], terahertz [64] and orthogonal time frequency space (OTFS) [65] wireless communication systems. In the context of wireless communication, where massive machine type communication involves a large number of connected devices, the demand for computationally efficient channel or parameter estimation algorithms like CoFBL becomes crucial [66].

Appendix A
Group sparse CCIR estimation

The complete likelihood ratio $\mathcal{L}\left(\boldsymbol{\Psi}_G|\widehat{\boldsymbol{\Psi}}_G^{(l-1)}\right)$ in E-step is derived as

$$\mathbb{E}\left[\log\left[p\left(\widetilde{\mathbf{Y}}|\mathbf{H}\right)\right]\right]+\mathbb{E}\left[\log\left[p\left(\mathbf{H};\boldsymbol{\Psi}_G\right)\right]\right]. \quad (48)$$

M-step: Next, one maximizes $\mathcal{L}\left(\mathbf{\Psi}_G|\widehat{\mathbf{\Psi}}_G^{(l-1)}\right)$ with respect to $\mathbf{\Psi}_G$ as

$$\widehat{\mathbf{\Psi}}_G^{(l)} = \arg\max_{\mathbf{\Psi}_G} \mathbb{E}\Big[\log\left[p\left(\mathbf{H};\mathbf{\Psi}_G\right)\right]\Big], \tag{49}$$

where we don't consider the term independent of $\mathbf{\Psi}_G$. Using (36), substituting $\log\left[p\left(\mathbf{H};\mathbf{\Psi}_G\right)\right]$, one obtains

$$\widehat{\mathbf{\Psi}}_G^{(l)} \equiv \arg\max_{\mathbf{\Psi}_G} \sum_{i=1}^{\frac{NMR}{d}} \left[-dK\log(\bar{\psi}_i) - \sum_{k=1}^{K} \frac{\mathbb{E}\{|\mathbf{h}_{n,m,k}(k)|^2\}}{\bar{\psi}_i}\right],$$

where we ignore the constant terms in the optimization that are independent of $\mathbf{\Psi}_G$. From the above equation, it can be readily observed that the optimization problem can be decoupled in each $\bar{\psi}_i$. Hence, the estimates $\widehat{\bar{\psi}}_i^{(l)}$ can be evaluated using

$$\widehat{\bar{\psi}}_i^{(l)} = \frac{1}{dK}\sum_{k=1}^{K} \mathbb{E}_{\mathbf{H}|\mathbf{Y};\widehat{\mathbf{\Psi}}_G^{(l-1)}}\Big[|\mathbf{h}_{n,m,k}(k)|^2\Big]. \tag{50}$$

The conditional expectation $\mathbb{E}_{\mathbf{H}|\mathbf{Y}}[.]$ can be evaluated using *a posteriori* pdf $p(\mathbf{H}|\mathbf{Y};\mathbf{\Psi}_G^{(l-1)})$ of $\mathbf{H}$, and is defined as $p\left(\mathbf{H}|\mathbf{Y};\widehat{\mathbf{\Psi}}_G^{(l-1)}\right) = \mathcal{CN}\left(\boldsymbol{\mathcal{M}}_G^{(l)},\mathbf{\Sigma}_G^{(l)}\right)$. The quantities $\mathbf{\Sigma}_G^{(l)} \in \mathbb{C}^{CGNt\times GNt}$ and $\boldsymbol{\mathcal{M}}_G^{(l)} \in \mathbb{C}^{CGNt\times GNt}$ are derived by substituting $\mathbf{\Psi} = \mathbf{\Psi}_G^{(l-1)}$ in Eq. (28), and $\mathbf{\Sigma} = \mathbf{\Sigma}_G^{(l)}$ in Eq. (27), respectively. Hence, $\mathbb{E}\Big[|\mathbf{h}_{n,m,k}(i)|^2\Big]$ can be evaluated as

$$\mathbb{E}\Big[|\mathbf{h}_{n,m,k}(i)|^2\Big] = \Big|\boldsymbol{\mathcal{M}}_G^{(l)}\left[\tilde{m},k\right]\Big|^2 + \mathbf{\Sigma}_G^{(l)}\left[\tilde{m},\tilde{m}\right],$$

which upon substituting into (50), yields the desired hyperparameter update of (38).

Appendix B
Joint sparse CCIR estimation

For the scenario with joint sparsity, the complete likelihood ratio $\mathcal{L}\left(\mathbf{\Psi}_J|\mathbf{\Psi}_J^{(l-1)}\right)$ in the E-step is

$$\mathbb{E}\Big[\log\Big[p\left(\widetilde{\mathbf{Y}}|\mathbf{H}\right)\Big]\Big] + \mathbb{E}\Big[\log\left[p\left(\mathbf{H};\mathbf{\Psi}_J\right)\right]\Big]. \tag{51}$$

In M-step, one maximizes $\mathcal{L}\left(\mathbf{\Psi}_J|\mathbf{\Psi}_J^{(l-1)}\right)$ with respect to $\mathbf{\Psi}$ as

$$\widehat{\mathbf{\Psi}}_J^{(l)} = \arg\max_{\mathbf{\Psi}_J} \mathbb{E}\Big[\log\left[p\left(\mathbf{H};\mathbf{\Psi}_J\right)\right]\Big], \tag{52}$$

ignoring the terms independent of $\mathbf{\Psi}_J$. Furthermore, using (41), and leaving out the terms independent of $\mathbf{\Psi}_J$, the hyperparameter covariance matrix estimate is

$$\widehat{\mathbf{\Psi}}_J^{(l)} \equiv \arg\max_{\mathbf{\Psi}_J} \sum_{i=1}^{R}\left[-NMK\log(\tilde{\psi}_i) - \sum_{n=1,m=1,k=1}^{N,M,K} \frac{\mathbb{E}\{|\mathbf{h}_{n,m,k}(i)|^2\}}{\tilde{\psi}_i}\right].$$

Similar to previous group sparse scenario, the hyperparameter estimates $\widehat{\tilde{\psi}}_i^{(l)}$ can be evaluated using

$$\widehat{\tilde{\psi}}_i^{(l)} = \frac{1}{NMK}\sum_{n=1}^{N}\sum_{m=1}^{M}\sum_{k=1}^{K} \mathbb{E}_{\mathbf{H}|\mathbf{Y};\widehat{\mathbf{\Psi}}_J^{(l-1)}}\Big[|\mathbf{h}_{n,m,k}(i)|^2\Big]. \tag{53}$$

The *a posteriori* pdf $p\left(\mathbf{H}|\mathbf{Y};\widehat{\mathbf{\Psi}}_J^{(l-1)}\right) = \mathcal{CN}\left(\boldsymbol{\mathcal{M}}_J^{(l)},\mathbf{\Sigma}_J^{(l)}\right)$ is used to evaluate condition expectation $\mathbb{E}_{\mathbf{H}|\mathbf{Y}}[.]$. Hence, $\mathbb{E}\Big[|\mathbf{h}_{n,m,k}(i)|^2\Big]$ can be evaluated as

$$\mathbb{E}\Big[|\mathbf{h}_{n,m,k}(i)|^2\Big] = \frac{1}{NMK}\sum_{n=1}^{N}\sum_{m=1}^{M}\sum_{k=1}^{K}\Big|\boldsymbol{\mathcal{M}}_J^{(l)}\left[\bar{m},k\right]\Big|^2 + \widetilde{\mathbf{\Sigma}}_J^{(l)}\left[\bar{m},\bar{m}\right],$$

which upon substituting into (53), yields the desired hyperparameter update of (42).

Appendix C
Joint-cum-group sparse CCIR estimation

For the scenario with joint-cum-group sparsity, in E-step one evaluates $\mathcal{L}\left(\mathbf{\Psi}_{JG}|\mathbf{\Psi}_{JG}^{(l-1)}\right)$ using

$$\mathbb{E}\Big[\log\Big[p\left(\widetilde{\mathbf{Y}}|\mathbf{H}\right)\Big]\Big] + \mathbb{E}\Big[\log\left[p\left(\mathbf{H};\mathbf{\Psi}_{JG}\right)\right]\Big]. \tag{54}$$

Furthermore, in M-step, one maximizes $\mathcal{L}\left(\mathbf{\Psi}_{JG}|\mathbf{\Psi}_{JG}^{(l-1)}\right)$ with respect to $\mathbf{\Psi}$ which can be mathematically represented as

$$\widehat{\mathbf{\Psi}}_{JG}^{(l)} = \arg\max_{\mathbf{\Psi}_{JG}} \mathbb{E}\Big[\log\left[p\left(\mathbf{H};\mathbf{\Psi}_{JG}\right)\right]\Big], \tag{55}$$

Furthermore, using (43), one can substitute $\log\left[p\left(\mathbf{H};\mathbf{\Psi}_{JG}\right)\right]$ above, one obtains

$$\widehat{\mathbf{\Psi}}_{JG}^{(l)} \equiv \arg\max_{\mathbf{\Psi}_{JG}} \sum_{i=1}^{R/n}\left[-NMK\log(\underline{\psi}_i) - \sum_{n=1,m=1,k=1}^{N,M,K} \frac{\mathbb{E}\{|\mathbf{h}_{n,m,k}(i)|^2\}}{\underline{\psi}_i}\right]. \tag{56}$$

Finally, the hyperparameter estimates $\widehat{\underline{\psi}}_i^{(l)}$ can be evaluated using

$$\widehat{\underline{\psi}}_i^{(l)} = \frac{1}{nNMK}\sum_{n=1}^{N}\sum_{m=1}^{M}\sum_{k=1}^{K} \mathbb{E}_{\mathbf{H}|\mathbf{Y};\widehat{\mathbf{\Psi}}_{JG}^{(l-1)}}\Big[|\mathbf{h}_{n,m,k}(i)|^2\Big].$$

The conditional expectation $\mathbb{E}_{\mathbf{H}|\mathbf{Y}}[.]$can be evaluating using *a posteriori* pdf $p\left(\mathbf{H}|\mathbf{Y};\widehat{\mathbf{\Psi}}_{JG}^{(l-1)}\right) = \mathcal{CN}\left(\boldsymbol{\mathcal{M}}_{JG}^{(l)},\mathbf{\Sigma}_{JG}^{(l)}\right)$. The matrices $\mathbf{\Sigma}_{JG}^{(l)} \in \mathbb{C}^{CGNt\times GNt}$ and $\boldsymbol{\mathcal{M}}_{JG}^{(l)} \in \mathbb{C}^{CGNt\times GNt}$ are derived by replacing $\mathbf{\Psi} = \mathbf{\Psi}_{JG}^{(l-1)}$ in Eq. (28), and $\mathbf{\Sigma} = \mathbf{\Sigma}_{JG}^{(l)}$ in Eq. (27), respectively. Finally, one obtains

$$\mathbb{E}\Big[|\mathbf{h}_{n,m,k}(i)|^2\Big] = \frac{1}{nNMK}\sum_{n=1}^{N}\sum_{m=1}^{M}\sum_{k=1}^{K}\Big|\boldsymbol{\mathcal{M}}_{JG}^{(l)}\left[\underline{m},k\right]\Big|^2 + \frac{1}{nNM}\sum_{n=1}^{N}\sum_{m=1}^{M}\widetilde{\mathbf{\Sigma}}_{JG}^{(l)}\left[\underline{m},\underline{m}\right],$$

which upon substituting into (56), yields the desired hyperparameter update of (45).

References

[1] K. P. Rajput, M. R. Bhavani Shankar, K. V. Mishra, M. Rangaswamy, and B. Ottersten, "CoFAR clutter channel estimation via sparse Bayesian learning," in *IEEE Radar Conference*, 2023, pp. 1–5.

[2] S. Haykin, "Cognitive radar: A way of the future," *IEEE Signal Processing Magazine*, vol. 23, no. 1, pp. 30–40, 2006.

[3] J. S. Bergin, J. R. Guerci, R. M. Guerci, and M. Rangaswamy, "MIMO clutter discrete probing for cognitive radar," in *IEEE Radar Conference*, 2015, pp. 1666–1670.

[4] J. R. Guerci, "Cognitive radar: A knowledge-aided fully adaptive approach," in *IEEE Radar Conference*, 2010, pp. 1365–1370.

[5] J. R. Guerci, R. M. Guerci, M. Ranagaswamy, J. S. Bergin, and M. C. Wicks, "CoFAR: Cognitive fully adaptive radar," in *IEEE Radar Conference*, 2014, pp. 0984–0989.

[6] K. L. Bell, C. J. Baker, G. E. Smith, J. T. Johnson, and M. Rangaswamy, "Fully adaptive radar for target tracking Part I: Single target tracking," in *IEEE Radar Conference*, 2014, pp. 0303–0308.

[7] ——, "Fully adaptive radar for target tracking Part II: Target detection and track initiation," in *IEEE Radar Conference*, 2014, pp. 0309–0314.

[8] A. E. Mitchell, J. L. Garry, A. J. Duly, G. E. Smith, K. L. Bell, and M. Rangaswamy, "Fully adaptive radar for variable resolution imaging," *IEEE Transactions on Geoscience and Remote Sensing*, vol. 57, no. 12, pp. 9810–9819, 2019.

[9] L. Úbeda Medina and J. Grajal, "Implementation of the fully adaptive radar framework: Practical limitations," in *IEEE Radar Conference*, 2017, pp. 0761–0766.

[10] S. Haykin, B. Currie, and S. Kesler, "Maximum-entropy spectral analysis of radar clutter," *Proceedings of the IEEE*, vol. 70, no. 9, pp. 953–962, 1982.

[11] L. Spafford, "Optimum radar signal processing in clutter," *IEEE Transactions on Information Theory*, vol. 14, no. 5, pp. 734–743, 1968.

[12] W. B. Lewis, "Sea clutter," in *Radar Handbook*, 3rd ed., M. I. Skolnik, Ed. McGraw-Hill, 2008.

[13] V. Bringi, K. V. Mishra, and M. Thurai, *Advances in weather radar Volume 2: Precipitation Science, Scattering and Processing Algorithms, Volume*. IET, 2024.

[14] J. B. Billingsley, *Low-angle radar land clutter: Measurements and empirical models*. IET, 2002.

[15] K. D. Ward, S. Watts, and R. J. Tough, *Sea clutter: Scattering, the K distribution and radar performance*. IET, 2006, vol. 20.

[16] G. P. Kulemin, *Millimeter-wave radar targets and clutter*. Artech House, 2003.

[17] T. Musha and M. Sekine, "Models of clutter," in *Advanced Radar Techniques and Systems*, G. Galati, Ed. Peter Peregrinus, 1993.

[18] S. Kay, "Optimal signal design for detection of Gaussian point targets in stationary Gaussian clutter/reverberation," *IEEE Journal of Selected Topics in Signal Processing*, vol. 1, no. 1, pp. 31–41, 2007.

[19] J. R. Guerci, J. S. Bergin, R. J. Guerci, M. Khanin, and M. Rangaswamy, "A new MIMO clutter model for cognitive radar," in *IEEE Radar Conference*, 2016, pp. 1–6.

[20] M. D. Greenberg, *Applications of Green's functions in science and engineering*. Dover Publications, 1971.

[21] S. Gogineni, M. Rangaswamy, J. R. Guerci, J. S. Bergin, and D. R. Kirk, "Estimation of radar channel state information," in *IEEE Radar Conference*, 2019, pp. 1–4.

[22] B. Kang, S. Gogineni, M. Rangaswamy, and J. R. Guerci, "Constrained maximum likelihood channel estimation for CoFAR," in *Asilomar Conference on Signals, Systems, and Computers*, 2020, pp. 1162–1166.

[23] B. Kang, S. Gogineni, M. Rangaswamy, J. R. Guerci, and E. Blasch, "Adaptive channel estimation for cognitive fully adaptive radar," *IET Radar, Sonar & Navigation*, 2021.

[24] S. Sedighi, M. R. B. Shankar, K. V. Mishra, and M. Rangaswamy, "Physics-based cognitive radar modeling and parameter estimation," in *IEEE Radar Conference*, 2022, pp. 1–6.

[25] S. Gogineni, J. R. Guerci, H. K. Nguyen, J. S. Bergin, D. R. Kirk, B. C. Watson, and M. Rangaswamy, "High fidelity RF clutter modeling and simulation," *IEEE Aerospace and Electronic Systems Magazine*, vol. 37, no. 11, pp. 24–43, 2022.

[26] S. S. Chen, D. L. Donoho, and M. A. Saunders, "Atomic decomposition by basis pursuit," *SIAM Review*, vol. 43, no. 1, pp. 129–159, 2001.

[27] I. F. Gorodnitsky and B. D. Rao, "Sparse signal reconstruction from limited data using FOCUSS: A re-weighted minimum norm algorithm," *IEEE Transactions on Signal Processing*, vol. 45, no. 3, pp. 600–616, 1997.

[28] D. Wipf and B. Rao, "Sparse Bayesian learning for basis selection," *IEEE Transactions on Signal Processing*, vol. 52, no. 8, pp. 2153–2164, 2004.

[29] D. P. Wipf and B. D. Rao, "An empirical Bayesian strategy for solving the simultaneous sparse approximation problem," *IEEE Transactions on Signal Processing*, vol. 55, no. 7, pp. 3704–3716, 2007.

[30] S. Saha, F. R. de Hoog, Y. I. Nesterets, R. K. Rana, M. Tahtali, and T. E. Gureyev, "Sparse Bayesian learning for EEG source localization," *arXiv preprint arXiv:1501.04621*, 2015.

[31] N. Hu, B. Sun, J. Wang, J. Dai, and C. Chang, "Source localization for sparse array using nonnegative sparse Bayesian learning," *Signal processing*, vol. 127, pp. 37–43, 2016.

[32] A. Mishra, V. Gupta, S. Dwivedi, A. K. Jagannatham, and P. K. Varshney, "Sparse Bayesian learning-based target imaging and parameter estimation for monostatic MIMO radar systems," *IEEE Access*, vol. 6, pp. 68 545–68 559, 2018.

[33] J. Fang, L. Zhang, and H. Li, "Two-dimensional pattern-coupled sparse Bayesian learning via generalized approximate message passing," *IEEE Transactions on Image Processing*, vol. 25, no. 6, pp. 2920–2930, 2016.

[34] X. Tan and J. Li, "Computationally efficient sparse Bayesian learning via belief propagation," *IEEE Transactions on Signal Processing*, vol. 58, no. 4, pp. 2010–2021, 2010.

[35] Q. Su and Y.-C. Wu, "Convergence analysis of the variance in Gaussian belief propagation," *IEEE Transactions on Signal Processing*, vol. 62, no. 19, pp. 5119–5131, 2014.

[36] M. Al-Shoukairi, P. Schniter, and B. D. Rao, "A GAMP-based low complexity sparse Bayesian learning algorithm," *IEEE Transactions on Signal Processing*, vol. 66, no. 2, pp. 294–308, 2018.

[37] C. M. Bishop and M. Tipping, "Variational relevance vector machines," in *ACM Conference on Uncertainty in Artificial Intelligence*, 2000, pp. 46–53.

[38] S. D. Babacan, M. Luessi, R. Molina, and A. K. Katsaggelos, "Low-rank matrix completion by variational sparse Bayesian learning," in *IEEE International Conference on Acoustics, Speech and Signal Processing*, 2011, pp. 2188–2191.

[39] D. Shutin, T. Buchgraber, S. R. Kulkarni, and H. V. Poor, "Fast adaptive variational sparse Bayesian learning with automatic relevance determination," in *IEEE International Conference on Acoustics, Speech and Signal Processing*, 2011, pp. 2180–2183.

[40] B. Worley, "Scalable mean-field sparse Bayesian learning," *IEEE Transactions on Signal Processing*, vol. 67, no. 24, pp. 6314–6326, 2019.

[41] H. Duan, L. Yang, J. Fang, and H. Li, "Fast inverse-free sparse Bayesian learning via relaxed evidence lower bound maximization," *IEEE Signal Processing Letters*, vol. 24, no. 6, pp. 774–778, 2017.

[42] A. Lin, A. H. Song, B. Bilgic, and D. Ba, "Covariance-free sparse Bayesian learning," *IEEE Transactions on Signal Processing*, vol. 70, pp. 3818–3831, 2022.

[43] C. Bekas, E. Kokiopoulou, and Y. Saad, "An estimator for the diagonal of a matrix," *Applied numerical mathematics*, vol. 57, no. 11-12, pp. 1214–1229, 2007.

[44] M. R. Hestenes, E. Stiefel *et al.*, "Methods of conjugate gradients for solving linear systems," *Journal of Research of the National Bureau of Standards*, vol. 49, no. 6, pp. 409–436, 1952.

[45] J. Guerci and E. Baranoski, "Knowledge-aided adaptive radar at DARPA: An overview," *IEEE Signal Processing Magazine*, vol. 23, no. 1, pp. 41–50, 2006.

[46] S. Pillai, H. Oh, D. Youla, and J. Guerci, "Optimal transmit-receiver design in the presence of signal-dependent interference and channel noise," *IEEE Transactions on Information Theory*, vol. 46, no. 2, pp. 577–584, 2000.

[47] C.-Y. Chen and P. P. Vaidyanathan, "MIMO radar space-time adaptive processing using prolate spheroidal wave functions," *IEEE Transactions on Signal Processing*, vol. 56, no. 2, pp. 623–635, 2008.

[48] E. Fishler, A. Haimovich, R. Blum, L. Cimini, D. Chizhik, and R. Valenzuela, "Spatial diversity in radars—models and detection performance," *IEEE Transactions on Signal Processing*, vol. 54, no. 3, pp. 823–838, 2006.

[49] H. L. Van Trees, *Detection, estimation, and modulation theory: Optimum array processing*. John Wiley & Sons, 2004.

[50] S. M. Kay, *Fundamentals of statistical signal processing: Estimation theory*. Prentice-Hall, 1993.

[51] RFView™. [Online]. Available: http://rfview.islinc.com.

[52] J. A. Tropp, A. C. Gilbert, and M. J. Strauss, "Algorithms for simultaneous sparse approximation. part I: Greedy pursuit," *Signal Processing*, vol. 86, no. 3, pp. 572–588, 2006, sparse Approximations in Signal and Image Processing. [Online]. Available: https://www.sciencedirect.com/science/article/pii/S0165168405002227

[53] S. Cotter, B. Rao, K. Engan, and K. Kreutz-Delgado, "Sparse solutions to linear inverse problems with multiple measurement vectors," *IEEE Transactions on Signal Processing*, vol. 53, no. 7, pp. 2477–2488, 2005.

[54] S. Cotter and B. Rao, "Sparse channel estimation via matching pursuit with application to equalization," *IEEE Transactions on Communications*, vol. 50, no. 3, pp. 374–377, 2002.

[55] I. Gorodnitsky and B. Rao, "Sparse signal reconstruction from limited data using FOCUSS: a re-weighted minimum norm algorithm," *IEEE Transactions on Signal Processing*, vol. 45, no. 3, pp. 600–616, 1997.

[56] J. Capon, "High-resolution frequency-wavenumber spectrum analysis," *Proceedings of the IEEE*, vol. 57, no. 8, pp. 1408–1418, 1969.

[57] P. Chen, Z. Cao, Z. Chen, and X. Wang, "Off-grid DOA estimation using sparse bayesian learning in mimo radar with unknown mutual coupling," *IEEE Transactions on Signal Processing*, vol. 67, no. 1, pp. 208–220, 2019.

[58] K. V. Mishra, M. Bhavani Shankar, B. Ottersten, and A. L. Swindlehurst, *Signal Processing for Joint Radar Communications*. Wiley-IEEE Press, 2024.

[59] D. Bao, G. Qin, and Y.-Y. Dong, "A superimposed pilot-based integrated radar and communication system," *IEEE Access*, vol. 8, pp. 11 520–11 533, 2020.

[60] Z. Gao, Z. Wan, D. Zheng, S. Tan, C. Masouros, D. W. K. Ng, and S. Chen, "Integrated sensing and communication with mmwave massive MIMO: A compressed sampling perspective," *IEEE Transactions on Wireless Communications*, vol. 22, no. 3, pp. 1745–1762, 2023.

[61] V. Bringi, K. V. Mishra, and M. Thurai, *Advances in weather radar Volume 1: Precipitation sensing platforms*. IET, 2024.

[62] ——, *Advances in weather radar Volume 3: Emerging applications*. IET, 2024.

[63] H. Tang, J. Wang, and L. He, "Off-grid sparse Bayesian learning-based channel estimation for MmWave massive MIMO uplink," *IEEE Wireless Communications Letters*, vol. 8, no. 1, pp. 45–48, 2019.

[64] J. Wu, S. Kim, and B. Shim, "Parametric sparse channel estimation for RIS-assisted terahertz systems," *IEEE Transactions on Communications*, vol. 71, no. 9, pp. 5503–5518, 2023.

[65] L. Zhao, W.-J. Gao, and W. Guo, "Sparse Bayesian learning of Delay-Doppler channel for OTFS system," *IEEE Communications Letters*, vol. 24, no. 12, pp. 2766–2769, 2020.

[66] X. Zhang, F. Labeau, L. Hao, and J. Liu, "Joint active user detection and channel estimation via bayesian learning approaches in MTC communications," *IEEE Transactions on Vehicular Technology*, vol. 70, no. 6, pp. 6222–6226, 2021.

Biographies

Kunwar Pritiraj Rajput received the B.E. degree in electronics and communication engineering from Jabalpur Engineering College, Jabalpur, India, in 2010; the M.Tech. degree in digital communication from Atal Bihari Vajpayee Indian Institute of Information Technology and Management, Gwalior, India, in 2013; and the Ph.D. degree from the Indian Institute of Technology Kanpur, Kanpur, India, in 2022. He is currently working as a Research Associate with SPARC group, SnT, University of Luxembourg, Kirchberg, Luxembourg. His research interests include decentralized and distributed parameter estimation in MIMO, massive MIMO, mmWave MIMO wireless sensor networks, sparse signal processing, and ISAC. He was given the Best Teaching Assistant (TA) award for the 5G wireless communication course at IIT Kanpur. He was also a Finalist for the Qualcomm Innovation Fellowship in 2022. He worked as a Vice Chair of the IEEE Signal Processing Society, Student Chapter Branch, IIT Kanpur.

Bhavani Shankar M. R. received Masters and Ph. D in Electrical Communication Engineering from Indian Institute of Science, Bangalore in 2000 and 2007 respectively. He was a Post Doc at the ACCESS Linnaeus Centre, Signal Processing Lab, Royal Institute of Technology (KTH), Sweden from 2007 to September 2009. He joined SnT in October 2009 as a Research Associate and is currently a Senior Research Scientist/ Assistant Professor at SnT leading the Radar Signal Processing activities. He was with Beceem Communications, Bangalore from 2006 to 2007 as a Staff Design Engineer working on Physical Layer algorithms for WiMAX compliant chipsets. He was a visiting student at the Communication Theory Group, ETH Zurich, headed by Prof. Helmut Bölcskei during 2004. Prior to joining Ph. D, he worked on Audio Coding algorithms in Sasken Communications, Bangalore as a Design Engineer from 2000 to 2001. He is currently the Chair of the IEEE Benelux joint chapter on communications and vehicular technology, serves as handling editor for EURASIP Journal on Advances in Signal Processing and is a member of the IEEE SPS SAM Technical Committee. He was a co-recipient of the 2014 Distinguished Contributions to Satellite Communications Award, from the Satellite and Space Communications Technical Committee of the IEEE Communications Society and co-author of the paper that received Special Mention for the Barry Carlton best paper award by IEEE TAES in 2023.

Kumar Vijay Mishra (S'08-M'15-SM'18) obtained a Ph.D. in electrical engineering and M.S. in mathematics from The University of Iowa in 2015, and M.S. in electrical engineering from Colorado State University in 2012, while working on NASA's Global Precipitation Mission Ground Validation (GPM-GV) weather radars. He received his B. Tech. summa cum laude (Gold Medal, Honors) in electronics and communication engineering from the National Institute of Technology, Hamirpur (NITH), India in 2003. He is with the United States DEVCOM Army Research Laboratory as Research Scientist at the Institute for Systems Research, The University of Maryland, College Park under the ARL-ArtIAMAS program; Technical Adviser to Singapore-based automotive radar start-up Hertzwell and Boston-based imaging radar startup Aura Intelligent Systems; and honorary Research Fellow at SnT - Interdisciplinary Centre for Security, Reliability and Trust, University of Luxembourg. Previously, he had research appointments at the Electronics and Radar Development Establishment (LRDE), Defence Research and Development Organisation (DRDO) Bengaluru; IIHR - Hydroscience & Engineering, Iowa City, IA; Mitsubishi Electric Research Labs, Cambridge, MA; Qualcomm, San Jose; and Technion - Israel Institute of Technology.

Dr. Mishra is the Distinguished Lecturer of the IEEE Communications Society (2023-2024), IEEE Aerospace and Electronic Systems Society (AESS) (2023-2024), IEEE Vehicular Technology Society (2023-2024), IEEE Geoscience and Remote Sensing Society (2024-2025), and IEEE Future Networks Initiative (2022). He is the recipient of the IET Premium Best Paper Prize (2021), IEEE T-AES Outstanding Editor (2021), U. S. National Academies Harry Diamond Distinguished Fellowship (2018-2021), American Geophysical Union Editors' Citation for Excellence (2019), Royal Meteorological Society Quarterly Journal Editor's Prize (2017), Viterbi Postdoctoral Fellowship (2015, 2016), Lady Davis Postdoctoral Fellowship (2017), DRDO LRDE Scientist of the Year Award (2006), NITH Director's Gold Medal (2003), and NITH Best Student Award (2003). He has received Best Paper Awards at IEEE MLSP 2019 and IEEE ACES Symposium 2019.

Dr. Mishra is Chair (2023-present) of the Synthetic Apertures Technical Working Group of the IEEE Signal Processing Society (SPS) and Vice-Chair (2021-present) of the IEEE Synthetic Aperture Standards Committee, which is the first SPS standards committee. He is the Chair (2023-2026) of the International Union of Radio Science (URSI) Commission C. He has been an elected member of three technical committees of IEEE SPS: SPCOM, SAM, and ASPS, and IEEE AESS Radar Systems Panel. He has been Senior Area Editor of IEEE Transactions on Signal Processing (2024-), Associate Editor of IEEE Transactions on Aerospace and Electronic Systems (2020-) and IEEE Transactions on Antennas and Propagation (2023-). He has been a lead/guest editor of several special issues in journals such as IEEE Signal Processing Magazine, IEEE Journal of Selected Topics in Signal Processing, IEEE Journal on Selected Areas in Communications, and IEEE Journal of Selected Topics in Applied Earth Observations and Remote Sensing. He is the lead co-editor of three books on radar: Signal Processing for Joint Radar-Communications (Wiley-IEEE Press, 2024), Next-Generation Cognitive Radar Systems (IET Press Radar, Electromagnetics & Signal Processing Technologies Series, 2024), and Advances in Weather Radar Volumes 1, 2 & 3 (IET Press Radar, Electromagnetics & Signal Processing Technologies Series, 2024). His research interests include radar systems, signal processing, remote sensing, and electromagnetics.

Muralidhar Rangaswamy (S'89, M'93, SM'98, F'2006) received the B.E. degree in Electronics Engineering from Bangalore University, Bangalore, India in 1985 and the M.S. and Ph.D. degrees in Electrical Engineering from Syracuse University, Syracuse, NY, in 1992. He is presently employed as the Technical Lead for Radar Sensing at the Sensors Directorate of the Air Force Research Laboratory (AFRL). Prior to this he has held industrial and academic appointments.

His research interests include radar signal processing, spectrum estimation, modeling non- Gaussian interference phenomena, and statistical communication theory. A common theme of his research in these areas is that of big data. A large class of radar signal processing problems incurs the curse of dimensionality, namely, the training data requirement and computational cost grow explosively with increasing dimensionality. Dr. Rangaswamy developed innovative techniques to address these challenges by using physics-based approaches and exploiting underlying structure in the data gained from a priori information. He has co-authored more than 300 refereed journal and conference record papers in the areas of his research interests. Additionally, he is a contributor to 10 books and is a co-inventor on 3 U.S. patents.

Dr. Rangaswamy served as the Technical Editor (Associate Editor-in-Chief) for Radar Systems in the IEEE Transactions on Aerospace and Electronic Systems (IEEE-TAES) from 2007-2015 and as Associate Editor for Radar Systems within the IEEE-TAES from 2004-2007. He was the Co-Editor-in-Chief for the Digital Signal Processing journal between 2005 and 2011. Dr. Rangaswamy was a member of the Senior Editorial Board of the IEEE Journal of Selected Topics in Signal Processing (Jan 2012-Dec 2014). He was a 2-term elected member of the sensor array and multichannel processing technical committee (SAM-TC) of the IEEE Signal Processing Society between January 2005 and December 2010 and served as a member of the Radar Systems Panel (RSP) in the IEEE-AES Society 2006-2019. He was the General Chairman for the 4th IEEE Workshop on Sensor Array and Multichannel Processing (SAM- 2006), Waltham, MA, July 2006. Dr. Rangaswamy has served on the Technical Committee of the IEEE Radar Conference series in a myriad of roles (Track Chair, Session Chair, Special Session Organizer and Chair, Paper Selection Committee Member, Tutorial Lecturer). He served as the Publicity Chair for the First IEEE International Conference on Waveform Diversity and Design, Edinburgh, U.K. November 2004. He served on the conference sub- committee of the RSP. He was the Technical Program Chairman for the 2014 IEEE Radar Conference.

He received the 2023 IEEE-USA Harry Diamond award, the 2023 Society of Asian Scientists and Engineers (SASE) Career Achievement Award, the NATO Scientific Excellence award in 2022, the IEEE-AESS Harry Rowe Mimno AES Magazine best paper award in 2021, the NATO SET Technical Panel Team Excellence award in 2021, the 2020 IEEE Dayton Section Fritz Russ memorial award, the 2019 Technical Cooperation Panel award from the Office of Secretary of Defense, the 2019 International Society for Information Fusion Jean-Pierre Le Cadre Best Paper award, 2013 IEEE Warren White Radar Award, the 2013 Affiliate Societies Council Dayton (ASC-D) Outstanding Scientist and Engineer Award, the 2007 IEEE Region 1 Award, the 2006 IEEE Boston Section Distinguished Member Award, and the 2005 IEEE-AESS Fred Nathanson memorial outstanding young radar engineer award. He received the 2012 and 2005 Charles Ryan basic research award from the Sensors Directorate of AFRL, in addition to more than 40 scientific achievement awards. He was elected as a Fellow of the IEEE in January 2006 for contributions to mathematical techniques for radar space-time adaptive processing. He has an h-index of 41 and i-10 index of 118. In 2016, he received a service recognition for his role as the Technical Editor for the IEEE Transactions on Aerospace and Electronic Systems. In 2024 he was ranked 807 out of 197000 (scientists in his field) by a Stanford University survey of

scientists worldwide who are in the top 2 % of their field.

Bjorn Ottersten (S'87–M'89–SM'99–F'04) received the M.S. degree in electrical engineering and applied physics from Linköping University, Linköping, Sweden, in 1986, and the Ph.D. degree in electrical engineering from Stanford University, Stanford, CA, USA, in 1990. He has held research positions with the Department of Electrical Engineering, Linköping University, the Information Systems Laboratory, Stanford University, the Katholieke Universiteit Leuven, Leuven, Belgium, and the University of Luxembourg, Luxembourg. From 1996 to 1997, he was the Director of Research with ArrayComm, Inc., a start-up in San Jose, CA, USA, based on his patented technology. In 1991, he was appointed Professor of signal processing with the Royal Institute of Technology (KTH), Stockholm, Sweden. Dr. Ottersten has been Head of the Department for Signals, Sensors, and Systems, KTH, and Dean of the School of Electrical Engineering, KTH. He is the founding Director for the Interdisciplinary Centre for Security, Reliability and Trust, University of Luxembourg. He is a recipient of the IEEE Signal Processing Society Technical Achievement Award, the EURASIP Group Technical Achievement Award, and the European Research Council (ERC) advanced research grant twice. He has co-authored journal papers that received the IEEE Signal Processing Society Best Paper Award in 1993, 2001, 2006, 2013, and 2019, and 9 IEEE conference papers best paper awards. He has been a board member of IEEE Signal Processing Society, the Swedish Research Council and currently serves of the boards of EURASIP and the Swedish Foundation for Strategic Research as well as on the ERC Scientific Council. Dr. Ottersten has served as Editor in Chief of EURASIP Signal Processing, and acted on the editorial boards of IEEE Transactions on Signal Processing, IEEE Signal Processing Magazine, IEEE Open Journal for Signal Processing, EURASIP Journal of Advances in Signal Processing and Foundations and Trends in Signal Processing. He is a fellow of IEEE, EURASIP, and AAIA.